Tradeoffs in Neural Variational Inference

Thesis

Ashwin D. D'Cruz

Supervisor: **Dr. Sebastian Nowozin**
Prof. Bill Byrne

Department of Engineering
University of Cambridge

This project proposal is submitted for the degree of
Master Of Philosophy

Hughes Hall October 2017

Declaration

I, Ashwin D. D'Cruz, of Hughes Hall, being a candidate for the MPhil in Machine Learning, Speech and Language Technology, hereby declare that this report and the work described in it are my own work, unaided except as may be specified below, and that the report does not contain material that has already been used to any substantial extent for a comparable purpose.

Total word count: 13 732

Ashwin D. D'Cruz
October 2017

Acknowledgements

I would like to thank Dr. Sebastian Nowozin from Microsoft Research Cambridge for proposing this project, helping me get started with Chainer, and constantly providing useful feedback throughout the course of this project.

I'm also thankful to Prof. Bill Byrne for his guidance and advice during this time.

A special mention goes out to the MLSALT cohort. This year would have been nowhere near as enjoyable without you. Thank you for your patience in explaining relatively easy concepts to this simple engineer, always being down to go bug hunting, and celebrating our victories with a pint or three.

I would like to thank my parents, Gerard and Adeline D'Cruz, whose support remained undiminished even over the distance. A shout out to my siblings, Nisha and Rushil; our holiday together definitely refreshed me for the final sprint. I'll never forget our walk from the forest. Last but not least, thank you Antrim for proof-reading my work and being interested enough in it, to the point of reading more machine learning books than I.

Abstract

Humans understand the world on an operational and causal level, allowing us to make accurate predictions about the consequences of our actions, and enabling us to plan. What would it take to endow artificial intelligence with similar capabilities? An important component is the ability to learn from observations, that is, to translate data into a model that has a higher level representation. Such representation abstracts away irrelevant variation but preserves important characteristics of the observation, thus enabling data-efficient learning for recognition, classification, and causal modeling. In machine learning, the field of unsupervised learning addresses the challenge of learning models from observations.

One recent advancement in this field has been the development of Variational Auto-Encoders (VAE) ([31], [54]). Since its inception, there have been several suggested improvements. While these works compare their results to the original VAE work, a thorough comparison between these improvements is lacking.

In this work, we present a thorough comparison between several selected improvements. We compare the variational log likelihood between these models on three datasets of varying complexity: MSRC-12 ([19]), MNIST ([37]), and celebA ([39]).

While variational lower bounds are often presented, most work often neglects to discuss model complexity and the associated training times and convergence rates. We compare the modeling times for these various approaches to provide practical guidelines regarding the trade-offs between the variational lower bound achieved and the run time required for training.

Finally, we contribute an extensive code repository implementing these state of the art machine learning techniques on the datasets mentioned. These are developed using the Chainer ([66]) framework. These implemented models are also available for use on other datasets.

Table of contents

List of figures

List of tables

Nomenclature

Acronyms / Abbreviations

ADGM	Auxiliary Deep Generative Model
AE	Auto-Encoder
BP	Back-propagation
DNN	Deep Neural Network
ELBO	Evidence Lower Bound
GPU	Graphics Processing Unit
IAF	Inverse Autoregressive Flow
IWAE	Importance Weighted Auto-Encoder
KL	Kullback-Leibler
MC	Monte Carlo
NN	Neural Network
ReLU	Rectified Linear Unit
SDGM	Skip Deep Generative Model
SGD	Stochastic Gradient Descent
SGVB	Stochastic Gradient Variational Bayes
VAE	Variational Auto-Encoder
VI	Variational Inference

Chapter 1

Introduction

1.1 Motivation

1.1.1 Unsupervised Learning

Unsupervised learning is a field of machine learning in which the machine attempts to discover structure and patterns in a dataset ([24]). In the case where the machine has to estimate the probability of a new data point x_n given some previous points $x_1, ..., x_{n-1}$, we can develop a model that is useful for outlier detection. Unsupervised learning is also useful within the context of representation learning : given some data, identify the underlying latent factors that explain the observations.

Representation learning is useful for many applications ([4]). Learned good representations can be used as inputs for supervised machine learning systems ([57]) such as speech recognition ([59]), object recognition ([34]), and natural language processing ([2]).

1.1.2 Variational Auto-Encoder

The applications outlined above provide a strong basis for research into representation learning. Recently, one approach to this has been the Variational Auto-Encoder (VAE) ([31], [54]). This is an efficient probabilistic deep learning method that has gained a lot of popularity recently. It is widely applied due to its ease of use and promising results ([17]).

The basic VAE model is shown in Figure 1.1. The generative network is moving from the latent distribution z to distribution x and is parametrized by θ as shown by the solid lines. To train the generative network, a second network called the inference network is built and this network is shown by the dashed line. Here we move from the distribution of data to the latent space with a network parametrized by ϕ. The two are optimized together using stochastic gradient descent (SGD). The quality of inference and the generative process are dependent on the accuracy of the inference network.

There have been several proposals on how to improve the inference network of the VAE which would improve the model's capabilities. While these improvements draw comparisons to the original VAE work, a thorough comparison between the different improvements is lacking in the community. This is the gap we seek to close with this work.

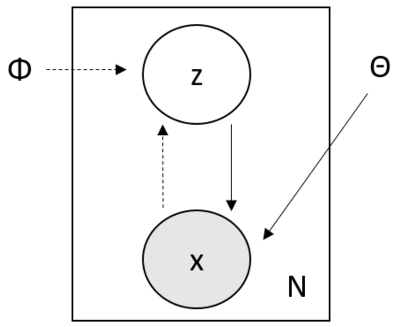

Fig. 1.1 VAE model.

1.1.3 Research Aims and Scope

Our work is concerned with a thorough quantitative evaluation of five modifications of the original VAE model on three datasets.
We compare the following works:

- Importance Weighted Auto-Encoder (IWAE) ([10])
- Auxiliary Deep Generative Model (ADGM) ([40])
- Skip Deep Generative Model (SDGM) ([40])
- Householder Flow Model ([67])
- Inverse Autoregressive Flow (IAF) Model ([33])

More information on these is provided in Chapter 3.

The following datasets are modeled:

- MSRC-12 ([19])

- MNIST ([37])
- celebA ([39])

More information on these is provided in Chapter 4.

The common metric used in comparing deep generative models is the variational lower bound; this metric is explained in Section 2.2 . We will also report the same metric. Additionally, we will investigate the modeling time taken by these various approaches. We will consider different aspects of this time metric. Of concern to us is how long the encoding and decoding process take as well as the update procedure for the parameters of the networks.

1.1.4 Organization

The remaining chapters are organized as follows:
Chapter 2 provides some background information on deep neural networks (DNNs) and variational inference (VI): two key building blocks in the development of VAEs. A review of VAE improvements and related work is presented in Chapter 3. The datasets used and methodology are detailed in Chapter 4. Chapter 5 discusses the results of our work and Chapter 6 proposes avenues for future work.

Chapter 2

Background

In this chapter, we will provide some background on the theory that forms the foundation for the rest of our work. In particular, we will cover the basics of deep neural networks (DNNs), including details about the training procedure and methods to augment this. We will also present a brief overview of variational inference (VI). Finally, we will show how these two concepts, DNNS and VI, meet in the form of Variational Auto-Encoders (VAEs).

For a more complete overview of DNNS, the reader is encouraged to look at the work of [58]. Similarly, please refer to [8] for a thorough review of VI.

2.1 Deep Neural Networks

For a long time, many machine learning techniques and algorithms required careful feature engineering from domain experts. Raw input would be processed through carefully constructed steps to obtain features that were thought to be useful for the task at hand. Examples of this include Mel-frequency cepstral coefficients for speech related tasks ([6, 22]) or SIFT features for computer vision ([5, 69]).

Within machine learning, representation learning allows a machine to automatically extract useful features from the raw input that can be used to solve specific tasks ([4]). Deep-learning methods are a form of representation learning. Specifically, neural networks (NNs) transform data from one representation into a more abstract one. DNNs do this repeatedly, learning a hierarchy of representations. Simple non-linear modules are used to transform one representation of the data into a higher, increasingly abstract representations ([38]). This begins with the raw input such as raw pixels of an image or raw waveforms and consecutive transformations could lead to features such as the class of the object within a image or the identity of a speaker. Given enough transformations, arbitrarily complex functions of the raw input can be learned.

The key aspect here is that the DNN is capable of automatically learning good representations by adjusting its parameters through the process of back-propagation. As this is a general training procedure, deep neural networks can be easily applied to a host of tasks with minimum domain expertise and manual feature crafting.

2.1.1 Notation

Figure 2.1 shows a DNN. This network has 4 input features, 4 output features and 2 hidden layers (each with 5 nodes). We adopt the similar notation to [21] and briefly outline it here.

A set of $\mathbf{x}^{(\mathbf{k})}$ form the inputs to layer k. $\mathbf{x}^{(\mathbf{1})}$ are the initial features from the dataset we are working with. At each layer, we denote the output as $\mathbf{y}^{(\mathbf{k})}$. Note that since the output from layer k are inputs to layer $(k+1)$, $\mathbf{y}^{(\mathbf{k})}$ can also be referred to as $\mathbf{x}^{(\mathbf{k+1})}$.

Figure 2.2 displays a more localized view of a single node. $\mathbf{w_i}$ refers to the weights at a given node and ϕ refers to the non-linearity applied to the output of the weights and inputs. There are various non-linearities that can be used and the choices we considered are given in Section 2.1.3.

At each layer, the following equation applies:

$$y_i^k = \phi(\mathbf{w_i}'\mathbf{x}^{(\mathbf{k})} + b_i) = \phi(\mathbf{z_i}^{(\mathbf{k})}) \tag{2.1}$$

Also of note is the number of parameters within particular DNN architectures. For a DNN such as that shown in Figure 2.1, the number of parameters can be calculated the following equation:

$$N = d \times N^{(1)} + K \times N^{(L)} + \sum_{k=1}^{L-1} N^{(k)} \times N^{(k+1)} \tag{2.2}$$

Where:

- L is the number of hidden layers
- $N^{(k)}$ is the number of nodes for layer k

- d is the input vector size, K is the output size

As seen, the number of parameters depends on both the width (number of nodes per layer) and depth of the network. [3, 35] showed that increasing the depth of a network is more favourable than increasing the width with regards to obtaining a more powerful network while minimizing the number of parameters used. More recent work by [68] has shown that this doesn't neccessarilly hold true for all types of network architectures. In our work, we will examine the differing widths and depths required to model the different datasets.

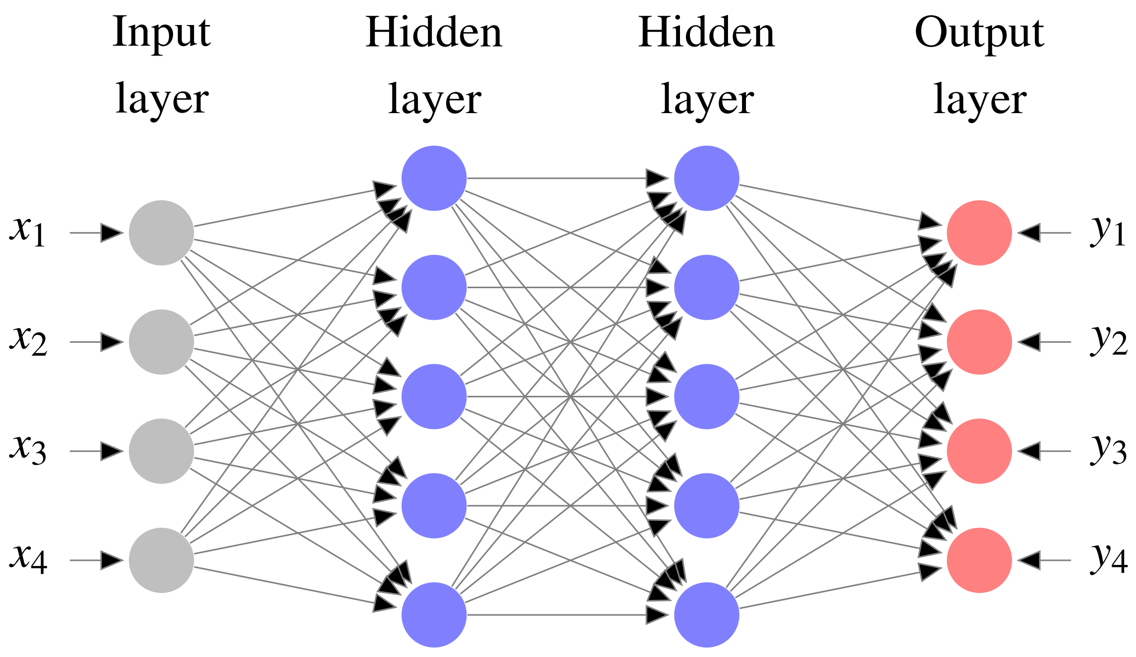

Fig. 2.1 Example of a deep neural network.

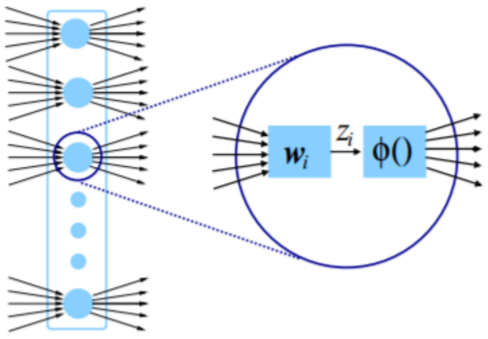

Fig. 2.2 Closer look at an individual neuron. Image taken from [21].

2.1.2 History

The idea of representing logical connections with structures mimicking biological neurons is not a new one. Early work in the 1940s such as [42] represented calculus operations with neural network architectures but these networks did not have the ability to learn. Following this, neural networks with simple training procedures were developed ([46], [55]) although these network architectures lacked depth.

Work by [26] examined the visual cortex of a cat and found that different cells picked up different features. Specifically, they categorized the cells into two general categories: simple and complex. The complex cells were more robust to spatial invariance. The work of [26] was significant in inspiring the *Neocognitron* ([20]), the first *deep* neural network. The hierarchy proposed by [20] was similar to the visual nervous system proposed by [26]. Additionally, [20] introduced the concept of convolutional neural networks (convnets) which allowed them to achieve spatial invariance, similar to the complex cells posited by [26]. In the present day, convnets are used in state of the art machine learning systems ([34, 48, 52])

In general, the weights of any arbitrary function can be updated through steepest descent in the weight space ([9]) using iterative applications of the chain rule. The process of propagating the error from the cost function from the final layer through the previous layers is known as back-propagation (BP). The work of [56] went a long way in popularizing the use of BP for the use of DNNs. BP is still the most widely used method for training DNNs. For more details on BP, please see [47, 56].

Following on, several improvements to optimization procedure have been suggested. We discuss the relevant improvements to our work in Section 2.1.3.

It is also important to mention the type of DNN developed by [56]: the Auto-Encoder (AE). In this DNN, an input vector is mapped to a lower dimensional representation (the encoding process) and then this new representation is used to reconstruct the original input (the decoding process). An example of what this network might look like is shown in Figure 2.3.

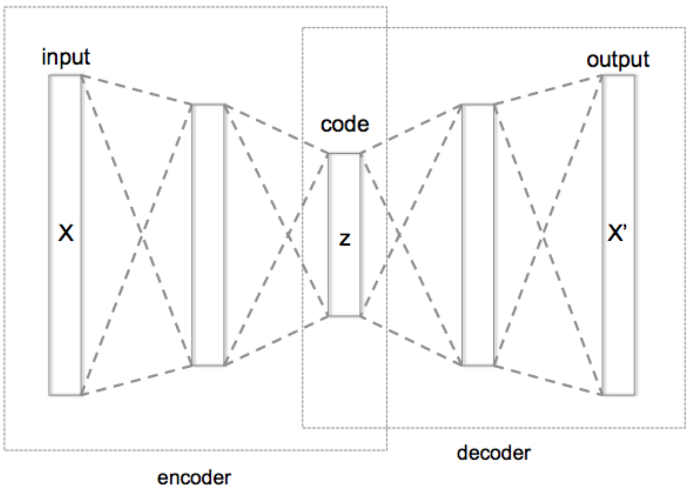

Fig. 2.3 Example of an auto-encoder. Image taken from [12].

This was important from a representation learning point of view but is of particular interest to our work as VAEs have a strong parallel to AEs.

While the work of [56] was vital in reviving research interest in DNNs, it was the achievement of DNNs in various competitions and industrial applications that would continue to drive development in this field. For example, MNIST records were set using DNNs by [61], [51], [14], and [13] in 2003, 2006, 2010, and 2012 respectively.

2.1.3 Improvements

Optimization

Adagrad ([18]) is a modification to the stochastic gradient descent (SGD) optimization procedure to produce an adaptive learning rate method. Under the standard SGD procedure, the same learning rate is used to update all parameters. With Adagrad however, each parameter obtains a specialised learning rate. Specifically, the more frequently a particular weight is updated, the smaller the learning rate for that weight. Weights that are infrequently updated are linked to sparse features. So in effect, Adagrad emphasizes learning from sparse features, believing them to be informative. The learning rate for all parameters tends towards 0 as a function of iterations and one of the disadvantages of Adagrad is that this often happens too early, halting the learning procedure before the model has reached an optimal point.

An improvement on this is *RMSProp* ([65]). Where Adagrad uses an average of squared gradients to control the decay rate, RMSProp uses a moving average of the squared gradients instead. By limiting the history considered, the decay isn't as aggressive and the learning procedure doesn't stop as early.

Building on this work is *Adam* ([30]). The squared gradients decay component of RMSprop is also known as second order momentum. Adam utilizes this but also uses first order momentum: a moving average of the gradient. This has been shown to lead to convergence in fewer iterations ([30]). In our work, we have chosen to use the Adam optimizer.

Activation Functions

The *rectified linear unit* or *ReLU* ([45]) non-linear activation function is commonly used in DNNs. It behaves in the following manner:

$$f(z) = max(0,z) \tag{2.3}$$

Compared to previous work such as the *sigmoid* or *tanh* activation functions, ReLu functions do not suffer from over-saturated activations. However, they can lead to 'dead' neurons if the input remains negative ([29]).

A recent proposal that overcomes this limitation is the *concatenated relu* or *CReLU* by [60]. Here, the activation is given by:

$$f(z) = (max(0,x), max(0,-x)) \tag{2.4}$$

This activation function is capable of utilizing both positive and negative Z (unlike the standard ReLU which returns 0 for negative inputs) while still having the property of being a non-saturating non-linearity. We use CReLU in our implementations.

Batch Normalization

Batch normalization ([27]) is a recently proposed technique to assist training in DNNs. It is common to normalize the input to a DNN to avoid any features having differing levels of impacts due to their respective scales. However, after passing through layers of a DNN, transformations might have undone this affect and the distributions of data at different depths of the network may be extremely disparate. [27] refer to this phenomenon as *internal covariate shift* and note that it causes difficulties with:

- Choosing effective learning rates.
- Parameter initialization.
- Saturating non-linearities.

[27] proposed a solution: normalizing the input at each layer after the weighted sum but before the non-linearities. The introduction of normalization at each layer of the network rather than only at the input level not only overcomes the difficulties mentioned earlier but was also shown to lead to improved final models ([27]).

2.2 Variational Inference

VI casts statistical inference problems as optimization problems ([28]). Specifically, when performing Bayesian inference, it may be intractable to use the exact posterior $p(z|x)$. Instead, an approximate posterior, $q_\phi(z|x)$, is chosen and the values for the parameters, ϕ, of this approximation are optimized to maximize a lower bound on the marginal likelihood. The set of equations we are interested in are shown below:

$$logp(x) - D_{KL}(q_\phi(z|x)||p(z|x)) = \mathbf{E}_{q_\phi}[logp(x,z) - logq_\phi(z|x)] \tag{2.5a}$$

$$logp(x) \geqslant \mathbf{E}_{q_\phi}[logp(x,z) - logq_\phi(z|x)] = \mathbf{L} \tag{2.5b}$$

Equation 2.5a relates the true log likelihood, $logp(x)$ to the true and approximate posteriors. Equation 2.5b depicts the Evidence Lower Bound (ELBO), **L**, which is the quantity we optimize as it doesn't involve the intractable posterior that was present in the Kullback–Leibler (KL) divergence term. Note that since the KL divergence is non-negative, the ELBO is a lower bound on the exact log likelihood.

When performing variational inference, we choose the family of distributions whose parameters we optimize. It is common to use mean field variational inference whereby the variables of the variational distribution are assumed to be independent. Due to this strong assumption, the variational family of distributions often does not contain the true posterior distribution ([7]). This is important to note for two reasons:

- While it is possible to find parameters ϕ such that $q_\phi(z|x)$ matches $p(z|x)$ exactly, we have stated that due to the strong assumption placed on the family of variational distributions, it is unlikely that the approximate posterior will match the true posterior.
- This weakness introduced by the family of variational distributions is what the suggested improvements we are examining seek to overcome.

2.3 Variational Auto-Encoder

VAEs combine DNNs and VI. Figure 2.4 depicts the construction of Equation 2.5b under the VAE framework. The approximate posterior, $q_\phi(z|x)$, is modeled using a DNN ([31, 54]). We also have a generative model $p_\theta(z,x)$ with parameters θ. The two are jointly optimized using VI techniques.

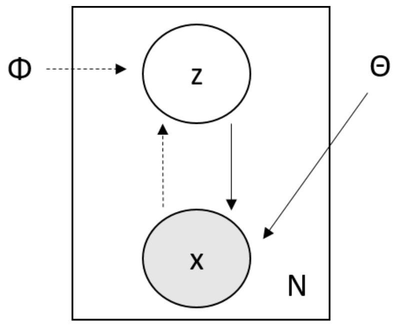

Fig. 2.4 VAE model.

One of the important contributions of [31, 54] was the development of the *reparametrization trick* and its subsequent use in the *Stochastic Gradient Variational Bayes* (SGVB) estimator. This practical gradient estimator does not suffer from high variance compared to previous work such as [50].

Chapter 3

Improvements and Related Work

In this chapter, we examine the proposed improvements to the Variational Auto-Encoder (VAE) in more depth.

3.1 Importance Weighted Auto-Encoder

The Importance Weighted Auto-Encoder (IWAE) was developed by [10]. Unlike most of the improvements we will discuss, the IWAE uses the same architecture as the standard VAE. Instead, the IWAE better utilizes the modeling capacity of the network by using a tighter log-likelihood lower bound or evidence lower bound (ELBO). This modified ELBO is derived from importance weighting and is shown in Equation 3.1a:

$$\mathbf{L}_k(x) = \mathbf{E}_{z_1,\ldots,z_k \sim q_\phi(z|x)} \left[log \frac{1}{k} \sum_{i=1}^{k} \frac{p_\theta(x, z_i)}{q_\phi(z_i|x)} \right] \tag{3.1a}$$

One of the variational assumptions is that the latent space is approximately factorial. The standard VAE objective heavily penalizes samples that don't adhere to this assumption. However, as the true posterior is unlikely to be approximately factorial, the standard VAE objective may be ignoring samples that are actually more likely under the true posterior. The IWAE relaxes this assumption of an approximately factorial posterior using importance sampling. It considers samples that don't adhere to this assumption and uses importance weighting to better take into account all samples from the approximate posterior, not just ones that satisfy the variational assumption. This relaxation on the sampling procedure allows a more flexible generative network to be trained. [10] focused on showing how this modified ELBO was strictly tighter than the standard VAE ELBO and showed how as more samples were used, the modified ELBO approached the true log likelihood. Recent work by [15] expanded on the work by [10] to show how using the IWAE objective was equivalent to using the standard VAE objective but with a more complex approximate posterior distribution that did not strictly adhere to the standard variational assumptions.

3.2 Auxiliary Deep Generative Model

Auxiliary Deep Generative Models (ADGMs) were developed by [40]. In this work, they focused on the semi-supervised task where datapoints x had labels y. For this task, the graphical model for the inference and generative networks of the ADGM are shown in Figure 3.1.

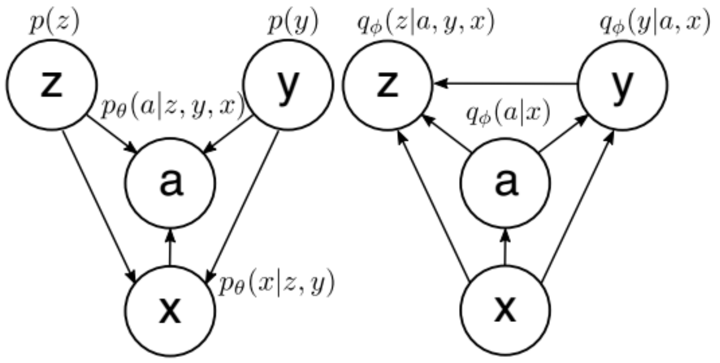

Fig. 3.1 ADGM graphical model. The model on the left is the generative network and the one of the right is the inference network. Image taken from [40].

The main contribution here is the introduction of the set of auxiliary latent variables, a. This auxiliary variable helps tie together the other variables in the network without requiring the latent space z to become significantly more complex. For the task we are interested in, unsupervised learning, the probabilistic model is similar to that shown in Figure 3.1 but without the inclusion of the labels y. In this task, we can see from the inference network that a acts as a feature extractor on x and that these additional features are used to develop a better latent space z. Specifically, [40] note that with this model the latent dimensions of z can be correlated through a. Note however that the generative procedure is still the same as what the standard VAE uses and the variable a is not necessary for sampling. It is only useful for the training procedure in developing better trained inference and generative networks.

3.3 Skip Deep Generative Model

Skip Deep Generative Models (SDGMs) were also developed by [40] are come about from a change to the ADGM. Specifically, in Figure 3.1, the arrow between a and x is reversed in the generative network but the inference network remains the same. Essentially, this pulls a into the generative process. In fact, what we now have is a 2 layer stochastic model where a is the added depth in the latent space. However, unlike the deep latent models used by [32, 54], here z feeds directly into x in the generative model through a skip connection. [40] note that this skip connection was crucial in allowing end-to-end training unlike [32] who could not achieve convergence with end-to-end training and had to resort to using layer wise training instead.

3.4 Inverse Autoregressive Flow

Inverse Autoregressive Flow (IAF) models were developed by [33]. At the core of their method are Gaussian autoregressive functions which in the past have been used for density estimation tasks ([23, 48, 49]). [33] show that such functions can be used for invertible non-linear transformations of the latent space, resulting in the IAF which is an example of a flow under the normalizing flow ([53, 63, 64]) framework.

Normalizing flows were first developed by [63, 64]. In these works, they proposed that a series of invertible mappings can be applied to simple probability distributions to obtain a more complex one. [53] utilized this idea for the purpose of enriching the approximate posterior in VAEs. Specifically, we begin with the approximate factorized posterior $\mathbf{z}_0$ and after T transformations, obtain a more flexible posterior, $\mathbf{z}_T$. The focus of [53] was on a specific parametrized family of transformations called *planar* flows. This transformation was given by Equation 3.2a:

$$\mathbf{f_t}(\mathbf{z_{t-1}}) = \mathbf{z_{t-1}} + \mathbf{u}h(\mathbf{w^T z_{t-1}} + b) \tag{3.2a}$$

In Equation 3.2a, $\mathbf{u}$ and $\mathbf{w}$ are vectors, b is a scalar and h is a non-linearity. Given these, one interpretation of the planar flow transformation is a multi layer perceptron bottleneck with a single unit ([33]). Due to this, this family of transformations is ill-suited to capture dependencies in a high dimensional latent space as a long series of transformations would be required.

The IAF model proposed by [33] avoids this issue because their inverse autoregressive functions can be parallelized. This allows better scaling to high dimensional latent spaces as the absence of a bottleneck means that fewer transformations are required to capture the dependencies between the dimensions. [33] note that given even a single IAF step, a Gaussian posterior with a diagonal covariance matrix can be transformed into one with a full covariance matrix.

3.5 Householder Flow

The Householder flow model developed by [67] is another example of a normalizing flow method. Within this framework, [67] state that their Householder flow method is an example of a *volume preserving* flow in which the Jacobian-determinants involved with the transformations equals 1. Hence the motivation for this method is that the Jacobian-determinants do not need to be explicitly calculated for each transformation, significantly reducing the computational complexity.

The core principle behind the Householder flow model is that full covariance matrices can be decomposed in the following way:

$$\Sigma = \mathbf{U}\mathbf{D}\mathbf{U}^{'} \tag{3.3a}$$

Where $\mathbf{U}$ is an orthogonal matrix and $\mathbf{D}$ is a diagonal matrix. If the covariance matrix of $\mathbf{z}_0$ corresponds to $\mathbf{D}$, then to achieve the full covariance matrix, all that is left is to model $\mathbf{U}$. [67] suggest the following method to model $\mathbf{U}$:

$$\mathbf{U} = \mathbf{H_T}\mathbf{H_{T-1}}...\mathbf{H_1} \tag{3.4a}$$

Where $\mathbf{T}$ is less than or equal to the dimensionality of $\mathbf{U}$ and $\mathbf{H_t}$ are Householder matrices.

The Householder transformation and matrix are shown in Equations 3.5a and 3.5b:

$$\mathbf{z_t} = \left(\mathbf{I} - \mathbf{2}\frac{\mathbf{v_t}\mathbf{v_t}^{'}}{||\mathbf{v_t}||^2}\right)\mathbf{z_{t-1}} \tag{3.5a}$$

$$= \mathbf{H_t}\mathbf{z_{t-1}} \tag{3.5b}$$

The initial Householder vector $\mathbf{v}_0$ is an output from the encoder network. Subsequent $\mathbf{v}_t$ are obtained by inputting $\mathbf{v}_{t-1}$ into a linear layer. Applications of the Householder flow help transform a factorized latent space into one with an approximate full covariance matrix, which is believed to be a closer approximation to the true posterior. It is worth noting that since Householder transformations are linear, they are cheaper to compute compared to non-linear transformations such as the IAF ([33]).

Chapter 4

Datasets and Experimental Procedure

We discuss the datasets used in this work, highlighting our motivation for using each one. Additionally, we also present our methodology.

4.1 MSRC-12

The MSRC-12 dataset ([19]) consists of sequences of human movements collected using the Kinect system. In this work, for clarity, we often refer to this dataset as the *Pose* dataset. Each datapoint consists of 60 points which form subsets of 3 points corresponding to 20 human joint locations. Each sequence is associated with 1 of 12 gestures. The dataset can be obtained from [44]. For the purpose of our work, we consider the individual frames of human movements with no regards for sequences or the gesture label. There are 702,551 frames in total. We split the frames into the following subsets:

- 321,275 samples for the training set
- 175,368 samples for the validation set
- 175,368 samples for the testing set

Figure 4.1 shows a few examples of these frames.

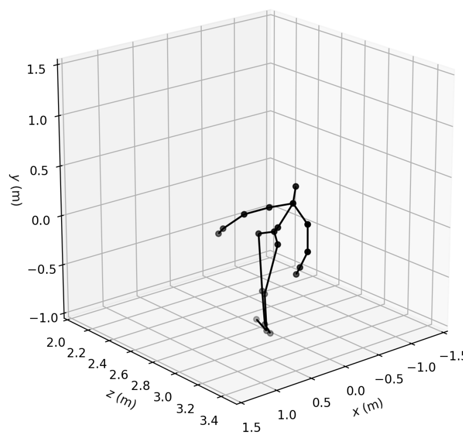

(a) Sample 1

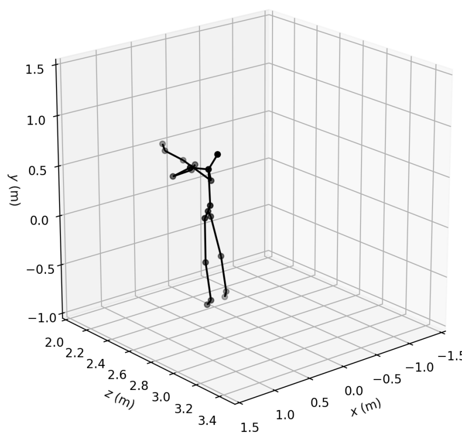

(b) Sample 2

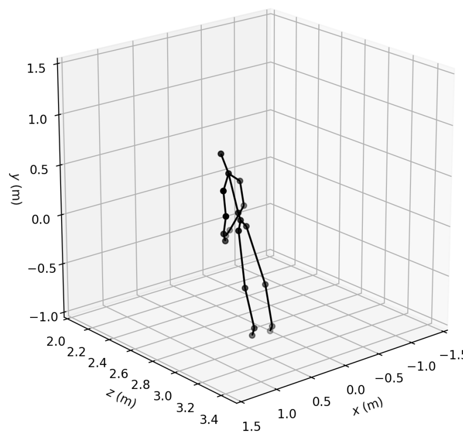

(c) Sample 3

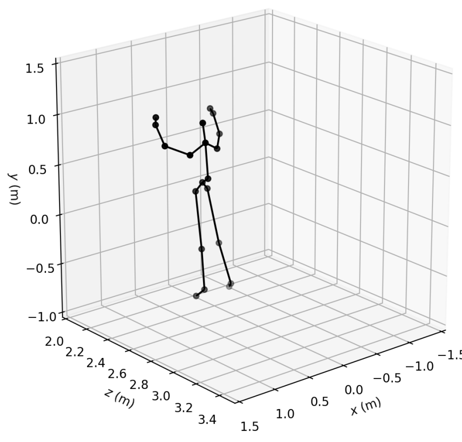

(d) Sample 4

Fig. 4.1 Pose data: Samples from the training dataset. Original datapoints are provided as a 60 dimensional vector. This was reshaped to give 20 joints, each as coordinate with 3 dimensions.

We chose to investigate this dataset as there is a lot of structure within a single frame. As points correspond to locations of humans joints, there is a strict order imposed on the location of joints relative to each other. The network would have to learn the general gestures while also learning this underlying structure and connectivity between the various joints. Furthermore, as this dataset is fairly new, we are interested in determining how well suited Variational Auto-Encoders (VAEs) are for this task.

4.2 MNIST

The MNIST dataset ([37]) has become a classic dataset in the machine learning community. It consists of 28x28, greyscale pixel images of handwritten digits, specifically the integers 0 through 9. For our work, we disregard the labels provided with each image as we are interested in an unsupervised learning task. There are 70,000 images in total which we split as such:

- 50,000 samples for the training set
- 10,000 samples for the validation set
- 10,000 samples for the testing set

Figure 4.2 shows a few examples of these images.

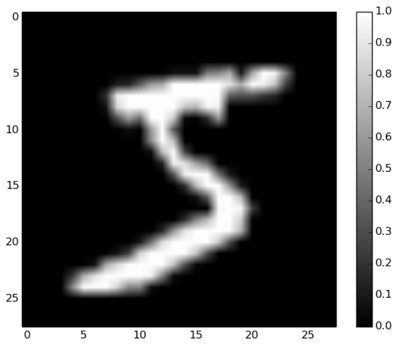

(a) Sample 1

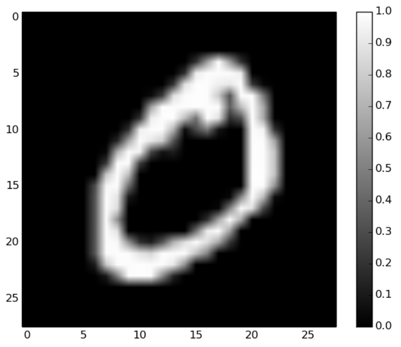

(b) Sample 2

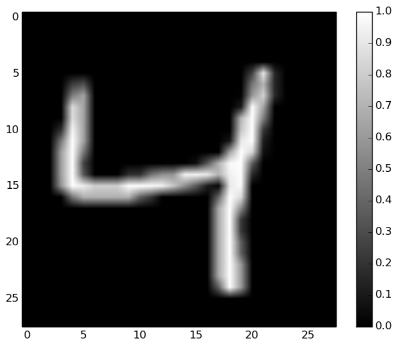

(c) Sample 3

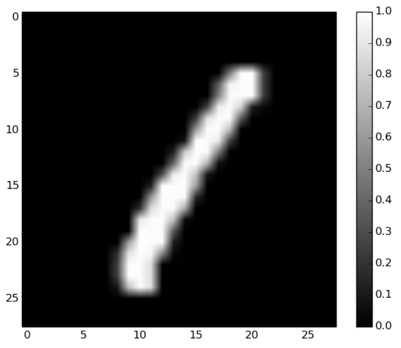

(d) Sample 4

Fig. 4.2 MNIST data: Samples from the training dataset. Images contain 28x28, grayscale pixels.

4.3 celebA

The celebA dataset ([39]) consists of more than 200,000 images of celebrity faces. For our work, we consider 200,000 of these which we split as follows:

- 100,000 samples for the training set
- 50,000 samples for the training set
- 50,000 samples for the training set

While each image comes with 40 different attributes, we ignore these as we are focused on an unsupervised learning task. [39] provides two versions of this dataset. One consists of the original data they gathered while with the other, the original data is first roughly aligned using a similarity transformation based on the eye locations before being scaled to be 218*178 pixels. These images contain 3 channels: red, green, and blue. Figure 4.3 shows a few images from this second version of this dataset. We chose these four images to showcase here as they highlight the variety present in the celebA dataset. Figure 4.3a shows a more 'casual' photo. In contrast, Figure 4.3b was taken in a more professional setting. Here, their face is directly facing the camera and while there is some detail in the background, it is not blurred. Figure 4.3c has a very distorted background that likely arose from the aligning and similarity transformation applied by [39]. Figure 4.3d is an example of where the photo was not taken front on.

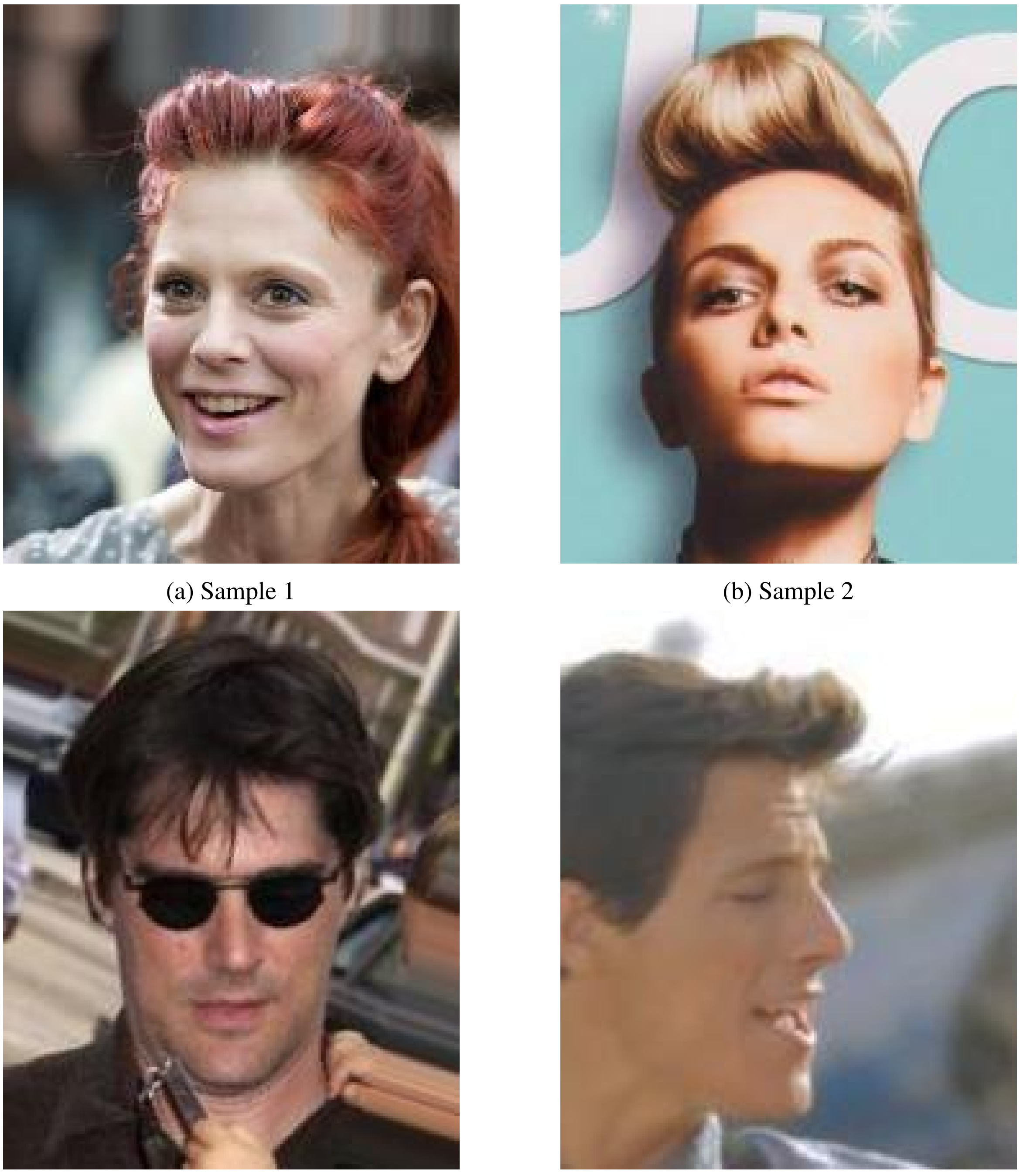
(a) Sample 1 (b) Sample 2

(c) Sample 3 (d) Sample 4

Fig. 4.3 celebA data: Samples from the training dataset. Images contain 218x178 pixels with three channels: red, green, and blue.

(a) Sample 1

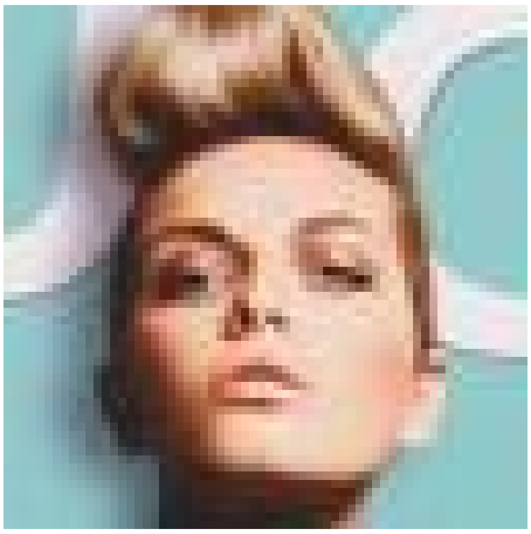
(b) Sample 2

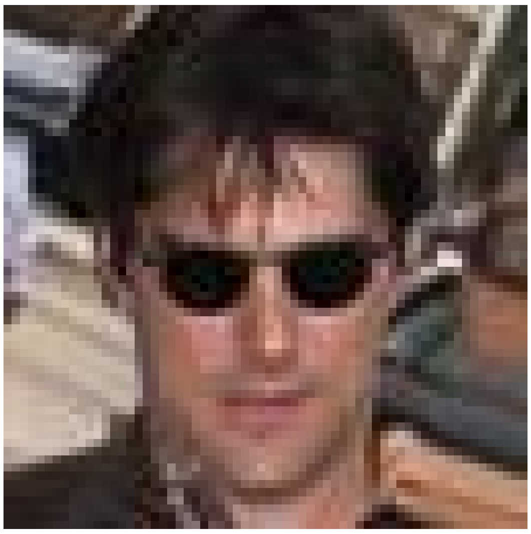
(c) Sample 3

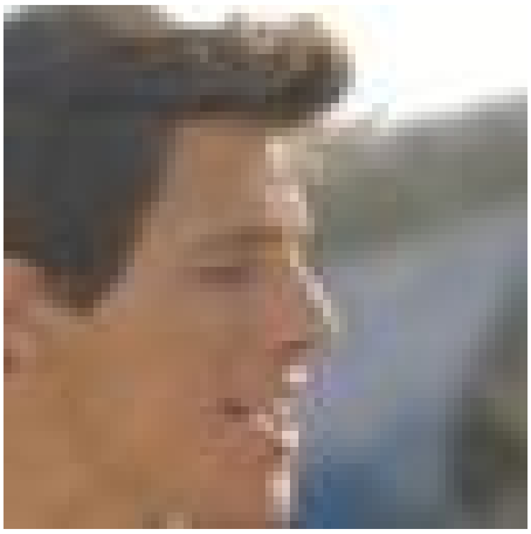
(d) Sample 4

Fig. 4.4 celebA data: Samples from the training dataset after we apply further cropping and scaling. Images contain 64x64 pixels with three channels: red, green, and blue.

We chose to work with the aligned and cropped version of the dataset. However, we decided to further pre-process the data as was done by other work ([11, 25, 36, 52]). We first cropped the image to be 178*178 before scaling it down to 64*64. Figure 4.4 shows a few images after our applied pre-processing. Information has been cropped from the top and bottom when moving from 218 to 178 pixels and the whole image is blurrier after down-sampling to 64x64 pixels.

We chose to examine this dataset as it was a fairly complex one. While it is also vision based like MNIST, the dimensionality here is larger and there are also 3 channels. Furthermore, these are facial images rather than hand-written digits and hence the underlying manifold should be more complex.

4.4 Methodology

We present the general methodology applied to each dataset while details of the network architecture for each dataset are given in Chapter 5.

For each dataset, we first chose one or more architectures to investigate. In this initial investigation, we focused on the convergence rate on the validation set; specifically, if the evidence lower bound (ELBO) decreases (indicating overfitting) and how many epochs were required to reach convergence. These investigations were carried out using the plain VAE model. With regards to network architecture, here are the basic hyper-parameters we focused on:

- Number of hidden units per hidden layer
- Dimensionality of the latent space
- Number of hidden layers in the encoder and decoder
- Batch size

In addition to this, we also focused on two additional settings: a warm up period for the Kullback–Leibler (KL) divergence term and the learning rate for the optimizer. We briefly describe the motivations for these.

4.4.1 Warm Up

Equation 2.5b can also be rewritten as the following:

$$\mathbf{L} = -KL(q_\phi(z|x)||p_\theta(z)) + \mathbf{E}_{q_\phi(z|x)}[p_\theta(z|x)] \tag{4.1a}$$

On the right hand side of the equation, the first term, the KL divergence term, can be considered a regularizer while the second term is called the reconstruction term. The regularizer term encourages the approximate posterior to model the prior whereas the reconstruction term rewards approximate posteriors that successfully reconstruct an input.

During the earlier stages of training, the optimizer may find it easier to focus on the KL term which shifts the approximate posterior to the prior. This may lead to latent units becoming inactive ([41]). [62] propose a fix to this called the *warm-up* scheme where the objective used is:

$$\mathbf{L} = -\beta KL(q_\phi(z|x)||p_\theta(z) + \mathbf{E}_{q_\phi(z|x)}[p_\theta(z|x)] \tag{4.2a}$$

During the first few training epochs or warm-up period, the parameter β is increased linearly from 0 to 1. This prevents the optimizer from immediately shifting the approximate posterior towards the prior.

Using this scheme adds a hyper-parameter: the number of epochs that make up the warm-up period. To tune this, we examined the changing ELBO, KL value, and reconstruction value during training in addition to samples produced by the generative network. We chose a warm-up period that allowed the reconstruction term to be optimized first, additionally informed by samples.

4.4.2 Learning rate

As mentioned in Section 2.1.3, we are using the Adam ([30]) optimizer in this work. [29] recommends using annealing with the learning rate to help the learning process. Using annealing, the search procedure starts aggressively but narrows down once it has, hopefully, found a good local minima. We decided to use an exponential annealing schedule given by:

$$\alpha = \alpha_0 \exp^{-kt} \tag{4.3a}$$

Where α is the current learning rate, α_0 is the initial learning rate, k is the decay hyper-parameter, and t is the epoch number. We first focus on choosing the appropriate α_0. When this value is too large, we can observe the ELBO bouncing around as the optimizer takes steps that are too large. Thus for α_0, we choose as large as possible a value while avoiding this bounce. We then note down how many epochs are required to reach convergence. Based on this value, we choose k such that the decay happens smoothly and not too rapidly over the maximum allowable epochs.

4.4.3 Evaluation

Once we determined a suitable architecture and number of training epochs, for each dataset, we trained 3 instances of each model. What differed between each model was the random initialization of network weights and the randomization of the order samples were processed every epoch. From these 3 models, we chose the model with the best validation ELBO and discarded the other two. We evaluate this best model on the held out test set. The ELBO of these best models for the validation and test set are reported in Chapter 5. Additionally, we record time measures for 100 epochs. These are averaged and reported in Chapter 5.

Chapter 5

Results

The results in this section are discussed per dataset before comparisons are drawn across the different datasets examined.

5.1 Pose Likelihood

5.1.1 Architecture

Our architecture was chosen based on advice from an author of [19] and is as follows:

Attribute	Value
Number of hidden units	512
Number of latent dimensions	16
Number of hidden layers in encoder network	4
Number of hidden layers in decoder network	4
Batch size	16384
Training epochs	1000
Warm up epochs	200
Initial learning rate	1e-4
Learning rate decay	3e-3

Table 5.1 Pose data: Network architecture.

5.1.2 Results

For each model, we report the best results on the validation set out of the 3 runs carried out. The best model from the 3 runs was then run on a held out test set and we also report the results on this.

Table 5.2 shows the results achieved by the Variational Auto-Encoder (VAE) and Importance Weighted Auto-Encoder (IWAE) model on the Pose validation dataset and Table 5.3 is related to the test dataset.

Number of Monte Carlo Samples	VAE		IWAE	
	Mean	SEM	Mean	SEM
1	126.05	0.06410	123.91	0.06479
2	127.05	0.06606	125.79	0.06291
5	136.00	0.06756	140.69	0.06396

Table 5.2 Pose data: average ELBO over the validation set (175,638 samples). We also report the standard error of the mean (SEM). Models examined are the standard VAE and IWAE.

Number of Monte Carlo Samples	VAE		IWAE	
	Mean	SEM	Mean	SEM
1	126.03	0.06415	125.80	0.06560
2	122.34	0.06348	130.81	0.06448
5	119.34	0.05478	122.91	0.05109

Table 5.3 Pose data: average ELBO over the test set (175,638 samples). We also report the standard error of the mean (SEM). Models examined are the standard VAE and IWAE.

Table 5.4 shows the results achieved by the Auxiliary Deep Generative Model (ADGM) and Skip Deep Generative Model (SDGM) model on the Pose validation dataset and Table 5.5 is related to the test dataset.

Number of Monte Carlo Samples	ADGM		SDGM	
	Mean	SEM	Mean	SEM
1	127.08	0.06686	142.97	0.06494

Table 5.4 Pose data: average ELBO over the validation set (175,638 samples). We also report the standard error of the mean (SEM). Models examined are the ADGM and SDGM.

Number of Monte Carlo Samples	ADGM		SDGM	
	Mean	SEM	Mean	SEM
1	127.08	0.06681	142.96	0.06500

Table 5.5 Pose data: average ELBO over the test set (175,638 samples). We also report the standard error of the mean (SEM). Models examined are the ADGM and SDGM.

Table 5.6 shows the results achieved by the Householder model on the Pose validation dataset and Table 5.7 is related to the test dataset.

Number of Transformations	Householder	
	Mean	SEM
1	116.35	0.06438
10	134.02	0.07007

Table 5.6 Pose data: average ELBO over the validation set (175,638 samples). We also report the standard error of the mean (SEM). Model examined is the Householder flow model. A single Monte Carlo sample was used for the expectation.

Number of Transformations	Householder	
	Mean	SEM
1	119.85	0.06787
10	133.03	0.06910

Table 5.7 Pose data: average ELBO over the test set (175,638 samples). We also report the standard error of the mean (SEM). Model examined is the Householder flow model. A single Monte Carlo sample was used for the expectation.

Table 5.8 shows the results achieved by the Inverse Autoregressive Flow (IAF) model on the Pose validation dataset and Table 5.9 is related to the test dataset.

Number of Transformations	IAF	
	Mean	SEM
1	125.79	0.06700
2	132.06	0.06815
3	135.14	0.06943
4	136.14	0.06937
8	146.06	0.07312

Table 5.8 Pose data: average ELBO over the validation set (175,638 samples). We also report the standard error of the mean (SEM). Model examined is the IAF model. A single Monte Carlo sample was used for the expectation.

Number of Transformations	IAF	
	Mean	SEM
1	125.78	0.06679
2	132.08	0.06814
3	135.82	0.06944
4	136.13	0.06930
8	146.04	0.07303

Table 5.9 Pose data: average ELBO over the test set (175,638 samples). We also report the standard error of the mean (SEM). Model examined is the IAF model. A single MC sample was used for the expectation.

5.1.3 Discussion

We first compare the VAE and IWAE. In this case, the network architecture is identical with the only difference being the objective function. The IWAE has a modified objective function that provides a tighter ELBO to the true log likelihood ([10]). Hence we expect to see that the IWAE performs better than the VAE, especially as the number of Monte Carlo (MC) samples is increased. Examining the validation set results shown in Table 5.2, we see that the IWAE has bigger gains in ELBO compared to the VAE when the number of samples is increased. This trend doesn't hold for the test set results, shown in Table 5.3. The VAE test results suggest that when the number of MC samples is increased, the architecture we chose was overfitting to the training and validation data since the ELBO for these latter two datasets continued to increase. The IWAE test results while slightly more erratic share some similarities. While using 2 MC samples worked better than 1, using 5 was worse than both cases indicating that with more samples, there was an issue with overfitting.

[10] noted that when a single MC sample is used, the original VAE ELBO formulation is reached and further supported this point in showing that their results were almost indistinguishable when comparing the VAE and IWAE with a single MC sample. We found that while the difference between our models was relatively small when using a single MC sample, there were not as close as those reported by [10]. We believe there are several explanations for this. First and foremost, we are examining a different dataset here. A more accurate comparison to [10] can be found in Section 5.2.3 in which we discuss how the models performed on the MNIST dataset. [10] also noted that due to the modified ELBO, the KL term could not be analytically obtained and hence the IWAE updates may have higher variance. Experimentally, they did not observe this. For our models, focusing on the case with a single MC sample, we see that the IWAE had a higher SEM for both the validation and test datasets. This would indicate that there is indeed higher variance. This effect is reduced when the number of MC samples is increased, at least when considering the validation dataset as we noted that there was an issue with overfitting during training leading to poor results on the test set.

In their original work, [10] considered the case of 1, 5, and 50 MC samples. We were limited to considering up to 5 MC samples due to the limitations of the compute resources available to us. Therefore we cannot say for certain that the worse performance by the IWAE compared to the VAE on the validation dataset for 1 and 2 MC samples is surprising. When 5 samples were used, the IWAE had a clearly better ELBO which indicates that the updated ELBO formulation and IWAE model may require a minimum number of MC samples before it can consistently outperform the VAE.

Next we consider the ADGM and SDGM model. We only considered the case of a single MC sample. The results on the validation set, shown in Table 5.4, are very similar to the test set, shown in Table 5.5, indicating that overfitting is not an issue here. [40] stated that the SDGM was a more flexible generative model compared to the ADGM and our results support that; for both the validation and test set, the SDGM outperforms the ADGM.

Looking at the results for the Householder model as shown in Tables 5.6 and 5.7, we observe that using more transformations was helpful in achieving significantly better results. This is in contrast to what was observed by [67] when working with the MNIST dataset. They noted that increasing the number of transformations did not lead to better performance. We believe that this is related to the complexity of the dataset being modeled and discuss this more in Section 5.2.3.

Considering the IAF results shown in Tables 5.8 and 5.9, we see that increasing the number of transformations led to better performance. This trend was also reported in the original work by [33]. The similarity between the results on the validation and test datasets indicates that these models did not suffer from overfitting. Additionally, the test results were slightly better than the validation results for all levels of tranformations. This indicates that the IAF model did very well in developing a flexible model that generalized well to unseen data.

Having considered different subsets of the models on hand, we now compare all the models previously discussed in this section. Table 5.10 shows the results obtained by these various models, ranked in order of decreasing ELBO for the validation dataset and Table 5.11 shows similar information for the test dataset.

Model	ELBO Mean
IAF (8 transformations)	146.06
SDGM	142.97
IWAE (5 MC samples)	140.69
IAF (4 transformation)	136.16
VAE (5 MC samples)	136.00
IAF (3 transformation)	135.14
Householder (10 transformations)	134.02
IAF (2 transformation)	132.06
ADGM	127.08
VAE (2 MC samples)	127.05
VAE (1 MC sample)	126.05
IAF (1 transformation)	125.79
IWAE (2 MC samples)	125.79
IWAE (1 MC sample)	123.91
Householder (1 transformation)	116.35

Table 5.10 Pose data: average ELBO over the validation set (175,638 samples). A single Monte Carlo sample was used for the expectation unless otherwise stated.

Model	ELBO Mean
IAF (8 transformations)	146.21
SDGM	142.96
IAF (4 transformation)	136.24
IAF (3 transformation)	135.82
Householder (10 transformations)	133.03
IAF (2 transformation)	132.08
IWAE (2 MC samples)	130.81
ADGM	127.08
VAE (1 MC sample)	126.03
IWAE (1 MC sample)	125.80
IAF (1 transformation)	125.78
IWAE (5 MC samples)	122.91
VAE (2 MC samples)	122.34
Householder (1 transformation)	119.85
VAE (5 MC samples)	119.34

Table 5.11 Pose data: average ELBO over the test set (175,638 samples). A single Monte Carlo sample was used for the expectation unless otherwise stated.

If we ignore the placements of the VAE and IWAE models, we see that the rankings are similar between the models for both the validation and test set. While both IAF and Householder models are examples of normalizing flows, we see that they have very different levels of transformative power on the latent space. For example, using a single Householder transformation leads to a very poor ELBO whereas using a single IAF transformation leads to a fairly good fit as indicated by the better ELBO that is comparable to many of the other models. We can draw a similar conclusion by noting that the best model for both the validation and test set was the IAF model with 8 transformations. In comparison, using 10 Householder transformations provided a strong ELBO but it was still outdone by IAF models with fewer transformations.

We also highlight that the SDGM model performs quite well as it was able to rank second without having to utilize transformations. While the ADGM performed well, it was outdone by models utilizing more than a single transformation. We believe that the reason the SDGM performs so well is that the latent space essentially has a depth of 2. This is explicitly stated in the modeling assumptions. An analogy can be drawn to the normalizing flow methods.

With normalizing flows, depth is added in the latent space through the transformations rather than through the explicit probabilistic model. Note that this isn't the case for the ADGM as in that case, the auxiliary variable doesn't lead to a 2-layer stochastic model since it is only used as a support variable to help link the other variables in the model.

Our work was focused on quantitative analysis and thus we did not rely on samples and reconstructions for analysis. We did however use these to ensure that models were training appropriately. Figure 5.1 shows an original Pose data-point and the reconstruction by several models. All the reconstructions seem viable except the Householder flow with 10 transformations as shown in Figure 5.1g which shows a large translation in the x dimension as well as changes in the elbow, wrist, and hand joints. However, this is just a single sample as hence we don't draw any strong conclusions, relying instead on the quantitative results.

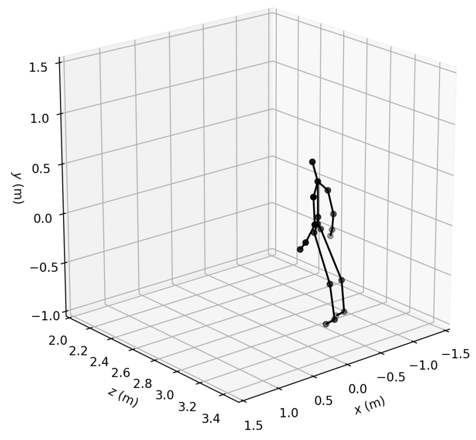

(a) Pose data: Original data-point

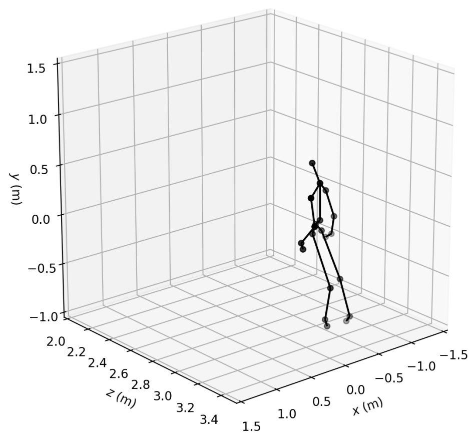

(b) Pose data: VAE reconstruction

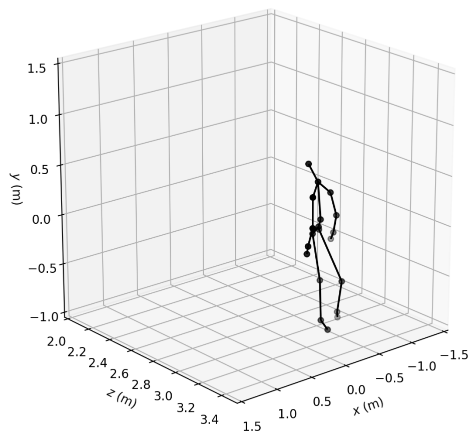

(c) Pose data: IWAE reconstruction

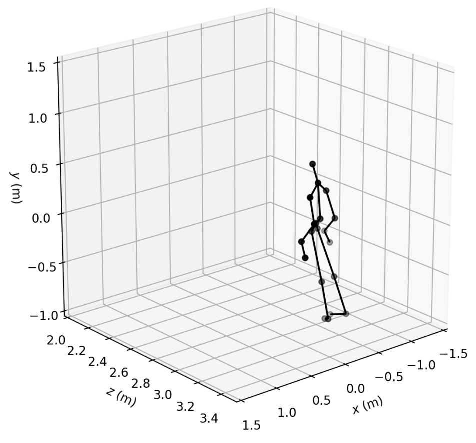

(d) Pose data: ADGM reconstruction

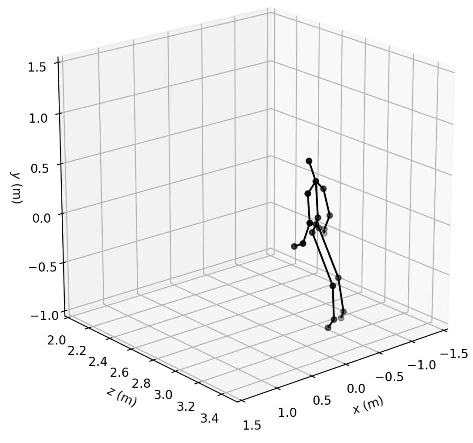

(e) Pose data: SDGM reconstruction

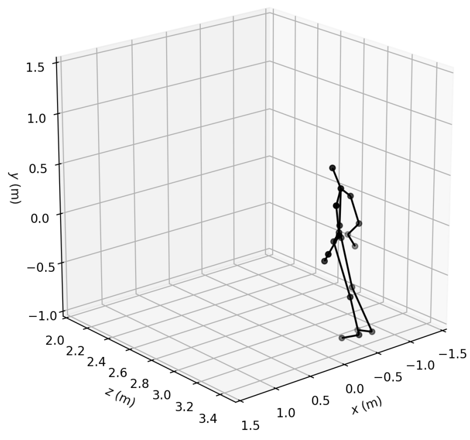

(f) Pose data: Householder flow (1 transformation) reconstruction

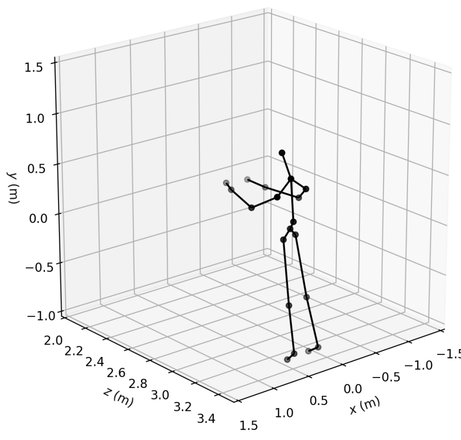

(g) Pose data: Householder flow (10 transformations) reconstruction

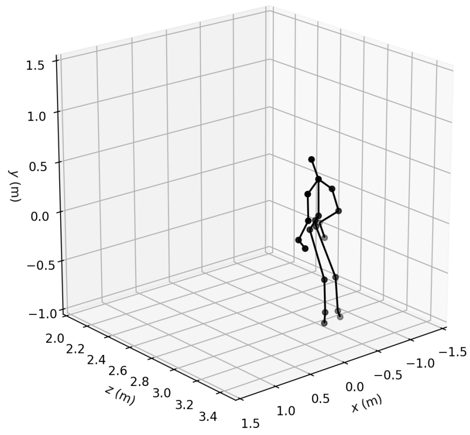

(h) Pose data: IAF (1 transformation) reconstruction

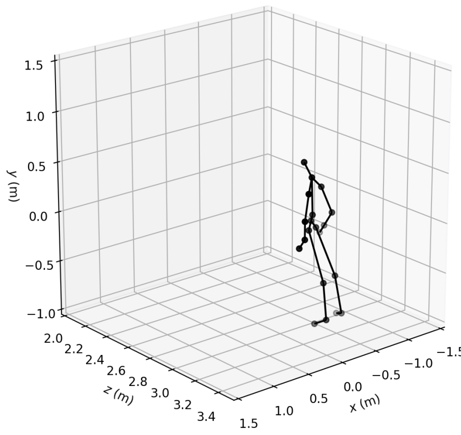

(i) Pose data: IAF (8 transformations) reconstruction

Fig. 5.1 Pose data: A single sample from the testing dataset and its various reconstructions with different models. All models only use a single Monte Carlo sample for expectations.

5.2 MNIST Likelihood

5.2.1 Architecture

To determine the best architecture to use, we considered the setups used by [10, 31, 33, 67]. The architecture we chose is as follows:

Attribute	Value
Number of hidden units	200
Number of latent dimensions	50
Number of hidden layers in encoder network	2
Number of hidden layers in decoder network	2
Batch size	4096
Training epochs	5000
Warm up epochs	200
Initial learning rate	1e-3
Learning rate decay	3e-3

Table 5.12 MNIST data: Network architecture.

5.2.2 Results

For each model, we report the best results on the validation set out of the 3 runs carried out. The best model from the 3 runs was then run on a held out test set and we also report the results on this. There were issues with the IAF model and thus results for that model are not included here.

Table 5.13 shows the results achieved by the VAE and IWAE model on the MNIST validation dataset and Table 5.14 is related to the test dataset.

Number of Monte Carlo Samples	VAE		IWAE	
	Mean	SEM	Mean	SEM
1	-99.50	0.2496	-99.44	0.2496
2	-99.39	0.2501	-98.14	0.2468
5	-99.21	0.2495	-96.85	0.2420

Table 5.13 MNIST data: average ELBO over the validation set (10,000 samples). We also report the standard error of the mean (SEM). Models examined are the standard VAE and IWAE.

Number of Monte Carlo Samples	VAE		IWAE	
	Mean	SEM	Mean	SEM
1	-98.96	0.2518	-98.81	0.2525
2	-97.78	0.2518	-97.42	0.2479
5	-98.56	0.2507	-96.15	0.2420

Table 5.14 MNIST data: average ELBO over the test set (10,000 samples). We also report the standard error of the mean (SEM). Models examined are the standard VAE and IWAE.

Table 5.15 shows the results achieved by the ADGM and SDGM model on the MNIST validation dataset and Table 5.16 is related to the test dataset.

Number of Monte Carlo Samples	ADGM		SDGM	
	Mean	SEM	Mean	SEM
1	-98.68	0.2509	-96.40	0.2480

Table 5.15 MNIST data: average ELBO over the validation set (10,000 samples). We also report the standard error of the mean (SEM). Models examined are the ADGM and SDGM.

Number of Monte Carlo Samples	ADGM		SDGM	
	Mean	SEM	Mean	SEM
1	-98.07	0.2523	-95.74	0.2493

Table 5.16 MNIST data: average ELBO over the test set (10,000 samples). We also report the standard error of the mean (SEM). Models examined are the ADGM and SDGM.

Table 5.17 shows the results achieved by the Householder model on the MNIST validation dataset and Table 5.18 is related to the test dataset.

Number of Transformations	Householder	
	Mean	SEM
1	-99.46	0.2518
10	-99.21	0.2502

Table 5.17 MNIST data: average ELBO over the validation set (10,000 samples). We also report the standard error of the mean (SEM). Model examined is the Householder flow model. A single Monte Carlo sample was used for the expectation.

Number of Transformations	Householder	
	Mean	SEM
1	-99.18	0.2533
10	-99.12	0.2543

Table 5.18 MNIST data: average ELBO over the test set (10,000 samples). We also report the standard error of the mean (SEM). Model examined is the Householder flow model. A single Monte Carlo sample was used for the expectation.

5.2.3 Discussion

Examining the results for the VAE and IWAE model, we note that using more samples improves the IWAE ELBO for both the validation and test datasets, as shown in Tables 5.13 and 5.14 respectively. Unlike the Pose dataset, the test set results followed a similar trend to the validation results indicating that overfitting was not an issue here. The use of more MC samples provided more benefit to the IWAE model compared to the VAE model which matches what was reported in [10]. The performance of the VAE model on the test dataset as the number of samples were increased indicate that the model does not benefit much from using more samples. We note that the exact ELBO values we obtain are different compared to those in [10]. We believe that the main reason for this is to do with the setup. For example: the specific architectures used, the number of training epochs utilized and the binarization scheme used. However, while this might mean that the models trained in [10] are better than the ones we have trained, our models are still useful for observing trends. Even within other literature, there is not an exact match between ELBO values (for example, the values reported by [10] are greater than that reported by [67] for the basic VAE model with a single

MC sample by approximately 7 ELBO points).

Comparing the ADGM and SDGM model, we see that similar to the Pose data, the SDGM model outperforms the ADGM model as shown in Tables 5.15 and 5.16. Looking at the two Householder setups examined, we see that using 10 transformations as opposed to just 1 provides some improvement but not by a large margin for both the validation and test set. This lack of significant improvement was also observed in the original work by [67].

Next we consider all the models discussed in this section. Table 5.19 shows the results obtained on the MNIST validation set, ranked in order of degrading ELBO and Table 5.20 reports similar data but for the test set.

Model	ELBO Mean
SDGM	-96.40
IWAE (5 MC samples)	-96.85
IWAE (2 MC samples)	-98.14
ADGM	-98.68
VAE (5 MC samples)	-99.21
Householder (10 transformations)	-99.21
VAE (2 MC samples)	-99.39
IWAE (1 MC sample)	-99.44
Householder (1 transformation)	-99.46
VAE (1 MC sample)	-99.50

Table 5.19 MNIST data: average ELBO over the validation set (10,000 samples). A single Monte Carlo sample was used for the expectation unless otherwise stated.

Model	ELBO Mean
SDGM	-95.74
IWAE (5 MC samples)	-96.15
IWAE (2 MC samples)	-97.42
VAE (2 MC samples)	-97.78
ADGM	-98.07
Householder (10 transformations)	-99.12
Householder (1 transformation)	-99.18
VAE (5 MC samples)	-98.56
IWAE (1 MC sample)	-98.81
VAE (1 MC sample)	-98.96

Table 5.20 MNIST data: average ELBO over the test set (10,000 samples). A single Monte Carlo sample was used for the expectation unless otherwise stated.

Similar to the results for the Pose data, the SDGM model outperforms the other models. We again believe that this is due to explicitly modeling the latent space with a depth of 2. For both the validation and test set, the basic VAE model with a single sample performs the worst. This is expected as it has the weakest latent representation and does not have a tighter bound like the IWAE model. We note that the range of ELBOs obtained here is much smaller than the results for the Pose data. This could be because the MNIST dataset is slightly easier to model and hence when more powerful models are used, the extra modeling capacity cannot be put to full use because the dataset is too simple to leverage it. This may also explain why the Householder model saw very little improvement when the number of transformations was increased. [67] also noted that using more transformations for the MNIST dataset yielded no significant improvement. However, as we showed in Section 5.1.3, for the Pose data, using more transformations yielded a large improvement. The lack of need for these more powerful models with richer latent spaces, specifically the Householder model, can also be justified by observing that the results obtained using the IWAE model with more than 1 MC sample were better than the Householder models for both the validation and test set.

Figure 5.2 shows an original sample from the MNIST test datasets and its reconstructions under some of the models.

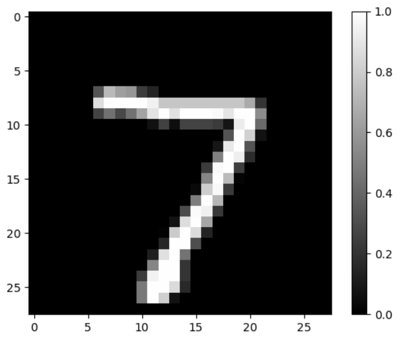
(a) MNIST data: Original sample

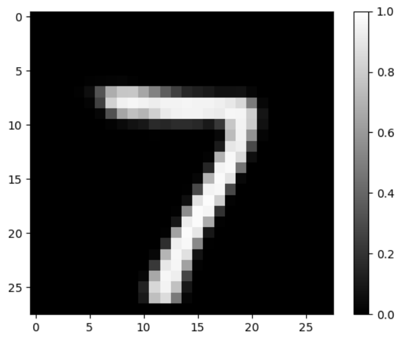
(b) MNIST data: VAE reconstruction

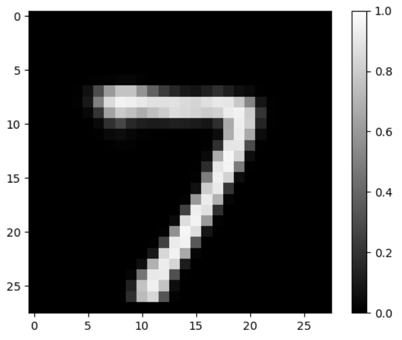
(c) MNIST data: IWAE reconstruction

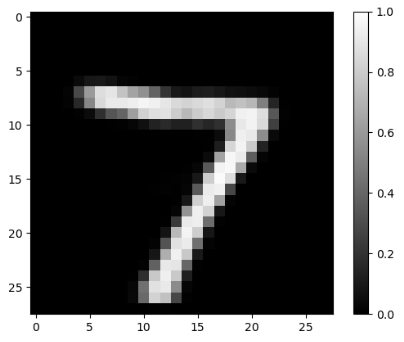
(d) MNIST data: Householder flow (1 transformation) reconstruction

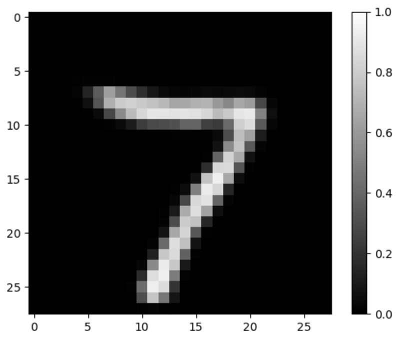
(e) MNIST data: ADGM reconstruction

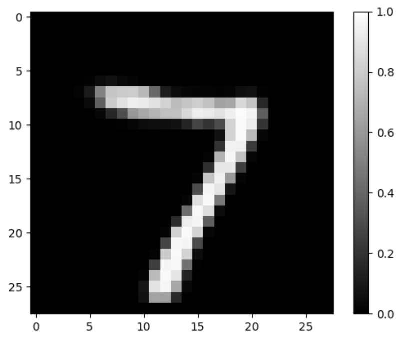
(f) MNIST data: SDGM reconstruction

Fig. 5.2 MNIST data: A single sample from the testing dataset and its various reconstructions with different models. All models only use a single Monte Carlo sample for expectations.

5.3 celebA Likelihood

5.3.1 Architecture

For this dataset, we did not have expert help as was the case for the Pose data or a lot of VAE-specific literature to rely on as was the case for MNIST. So we ran a separate set of experiments to determine the best architecture. Specifically, we focused on these hyper-parameters:

- Number of hidden units in each hidden layer
- Number of dimensions in the latent space
- Number of hidden layers in encoder and decoder network

Figure 5.3 shows the convergence plots for some of the cases we considered. To decide which values to investigate, we considered previous work on the celebA dataset ([1, 11, 43]). The decreasing ELBO when 3 hidden layers were used in conjunction with 512 hidden units in the encoder and decoder network show an issue with overfitting. Based on these experiments, we chose the following architecture:

Attribute	Value
Number of hidden units	512
Number of latent dimensions	256
Number of hidden layers in encoder network	2
Number of hidden layers in decoder network	2
Batch size	4096
Training epochs	1000
Warm up epochs	0
Initial learning rate	1e-3
Learning rate decay	0

Table 5.21 celebA data: Network architecture.

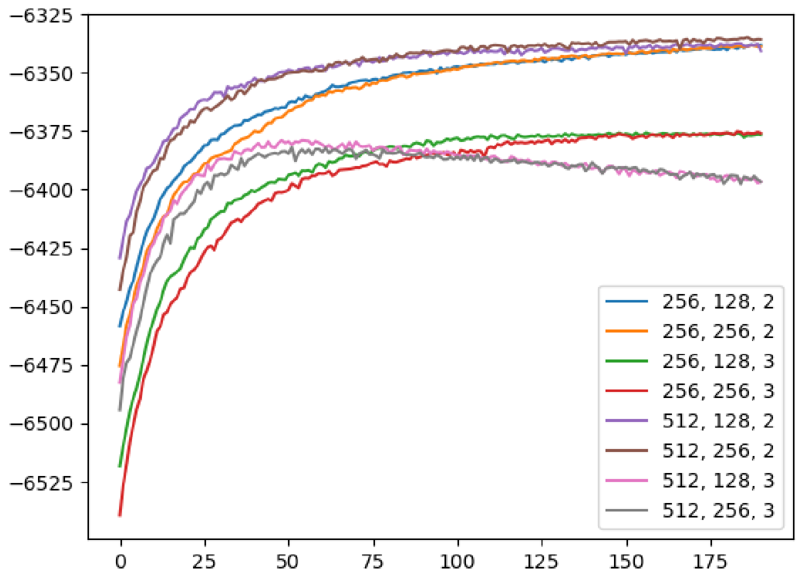

Fig. 5.3 celebA data: ELBO on the validation set for various network architectures. The legend is (number of hidden units per layer, number of dimensions in the latent space, number of hidden layer in the encoder and decoder). 1000 training epochs were run but the validation ELBO was only recorded every 5 epochs which is why the x-axis has a much smaller range. Additionally, we omit the results from the first 50 training epochs as these values were very small and prevented us from properly viewing the trends during later epochs.

Additionally, we included batch normalization with this dataset as it reduced the convergence rate by a factor of 5. We did not utilize warm-up or annealing the learning rate for this dataset as we were satisfied with the performance of the models without them.

5.3.2 Results

For each model, we report the best results on the validation set out of the 3 runs carried out. The best model from the 3 runs was then run on a held out test set and we also report the results on this. There were issues with the IAF model and thus results for that model are not included here.

Table 5.22 shows the results achieved by the VAE and IWAE model on the celebA validation dataset and Table 5.23 is related to the test dataset.

Number of Monte Carlo Samples	VAE		IWAE	
	Mean	SEM	Mean	SEM
1	-6336.33	4.33528	-6336.36	4.33468
2	-6335.54	4.33422	-6325.68	4.33758
5	-6334.39	4.33517	-6317.55	4.34009

Table 5.22 celebA data: average ELBO over the validation set (50,000 samples). We also report the standard error of the mean (SEM). Models examined are the standard VAE and IWAE.

Number of Monte Carlo Samples	VAE		IWAE	
	Mean	SEM	Mean	SEM
1	-6331.26	4.32211	-6330.70	4.32262
2	-6330.17	4.32264	-6320.38	4.32593
5	-6329.27	4.32154	-6312.24	4.32703

Table 5.23 celebA data: average ELBO over the test set (50,000 samples). We also report the standard error of the mean (SEM). Models examined are the standard VAE and IWAE.

Table 5.24 shows the results achieved by the ADGM and SDGM model on the celebA validation dataset and Table 5.25 is related to the test dataset.

Number of Monte Carlo Samples	ADGM		SDGM	
	Mean	SEM	Mean	SEM
1	-6337.12	4.33327	-6316.63	4.33521

Table 5.24 celebA data: average ELBO over the validation set (10,000 samples). We also report the standard error of the mean (SEM). Models examined are the ADGM and SDGM.

Number of Monte Carlo Samples	ADGM		SDGM	
	Mean	SEM	Mean	SEM
1	6331.93	4.32050	-6311.40	4.32312

Table 5.25 celebA data: average ELBO over the test set (50,000 samples). We also report the standard error of the mean (SEM). Models examined are the ADGM and SDGM.

Table 5.26 shows the results achieved by the Householder model on the celebA validation dataset and Table 5.27 is related to the test dataset.

Number of Transformations	Householder	
	Mean	SEM
1	-6336.48	4.33773
10	-6337.99	4.33879

Table 5.26 celebA data: average ELBO over the validation set (50,000 samples). We also report the standard error of the mean (SEM). Model examined is the Householder flow model. A single Monte Carlo sample was used for the expectation.

Number of Transformations	Householder	
	Mean	SEM
1	-6330.94	4.23480
10	-6333.25	4.32553

Table 5.27 celebA data: average ELBO over the test set (50,000 samples). We also report the standard error of the mean (SEM). Model examined is the Householder flow model. A single Monte Carlo sample was used for the expectation.

5.3.3 Discussion

For this dataset, we will move straight to comparing the models overall as the trends shown in the individual Tables were very similar to that discussed with the MNIST dataset. Table 5.28 shows the results obtained on the celebA validation set, ranked in order of worsening ELBO and Table 5.29 reports similar results but for the test set.

Model	ELBO Mean
SDGM	-6316.63
IWAE (5 MC samples)	-6317.55
IWAE (2 MC samples)	-6325.68
VAE (5 MC samples)	-6334.39
VAE (2 MC samples)	-6335.54
VAE (1 MC sample)	-6336.33
IWAE (1 MC sample)	-6336.36
Householder (1 transformation)	-6336.48
ADGM	-6337.12
Householder (10 transformations)	-6337.99

Table 5.28 celebA data: average ELBO over the validation set (50,000 samples). A single Monte Carlo sample was used for the expectation unless otherwise stated.

Model	ELBO Mean
SDGM	-6311.40
IWAE (5 MC samples)	-6312.24
IWAE (2 MC samples)	-6320.38
VAE (5 MC samples)	-6329.27
VAE (2 MC samples)	-6330.17
IWAE (1 MC sample)	-6330.70
Householder (1 transformation)	-6330.94
VAE (1 MC sample)	-6331.26
ADGM	-6331.93
Householder (10 transformations)	-6333.25

Table 5.29 celebA data: average ELBO over the test set (50,000 samples). A single Monte Carlo sample was used for the expectation unless otherwise stated.

As was the case for the previous datasets, the SDGM model outperforms the other models investigated here. The most surprising results are perhaps the performance of the ADGM and Householder (with 10 transformations) model. For both the validation and test set, these model perform worse than the basic VAE model. We believe that this is because this dataset is the most complex and hence some models require more fine-tuning than others. If this is the case, then the SDGM, IWAE, and VAE models have an advantage in that they are able to perform relatively well even without this fine tuning that the ADGM and Householder models may require.

While the celebA dataset is clearly more difficult to model, it does provide a better opportunity to compare models compared to the MNIST dataset. While the order of magnitude is different, the range of ELBO values for the celebA dataset is much larger than MNIST which helps comparisons between the different models. The Pose dataset is the best option as its order of magnitude, for ELBO values, is smaller than celebA and comparable to MNIST while the range of ELBO values obtained is the largest of all 3 datasets.

While the results from the architecture experiments showed that we were not overfitting and the ELBO results discussed previously indicated that different models were achieving differing fits to the data, a qualitative analysis indicated that there were some issues with our models for the celebA dataset. Figure 5.4 shows reconstructions of a sample from the celebA test dataset under our models. However, we found that the images shown appeared as the reconstruction for a range of test dataset inputs. This indicates that the models are centered around a 'generic' face that contains traits common to the dataset when it comes to reconstructing an image. While our architecture experiments indicated that a more powerful model would be overfitting, these images indicate that our model still lacks capacity for image reconstruction. One of the main differences of our work to previous works ([1, 11, 43]) is that we did not used convolutional layers. Thus the most likely explanation is that the features we were extracting from the image with our encoder network were insufficient for completely modeling the underlying manifold. However, these models did learn some of the necessary traits of the celebA dataset required for image generation. Figure 5.5 shows images obtained by random sampling from the generative network. As we can see, in this instance, we are not limited to the same image. The variety here indicates that facial attributes were learned and these models may be suitable for some generative tasks. The sample from the SDGM model indicates that this model has some issues but the ELBO associated with the validation and testing set for this model were reassuring. The images in Figure 5.4 indicate that for reconstruction purposes, we need to reexamine our model architectures.

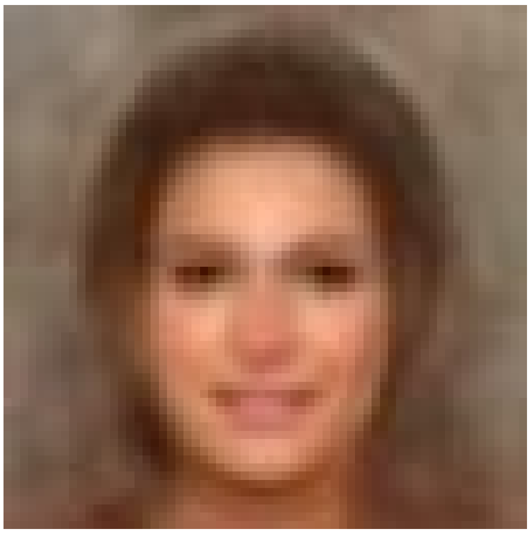
(a) celebA data: VAE reconstruction

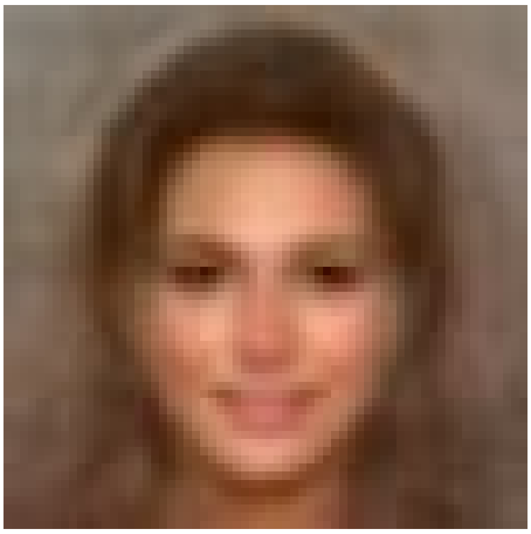
(b) celebA data: IWAE reconstruction

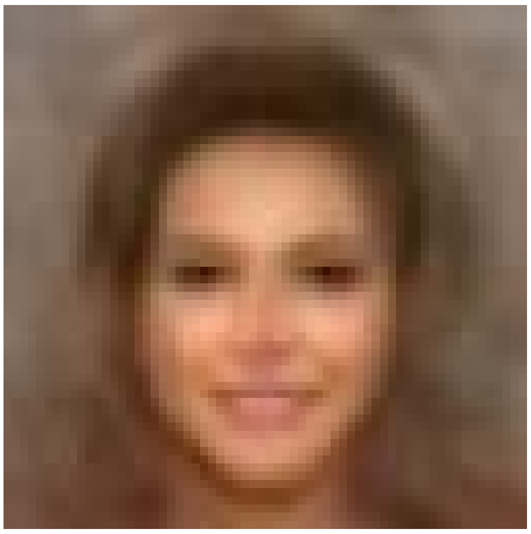
(c) celebA data: ADGM reconstruction

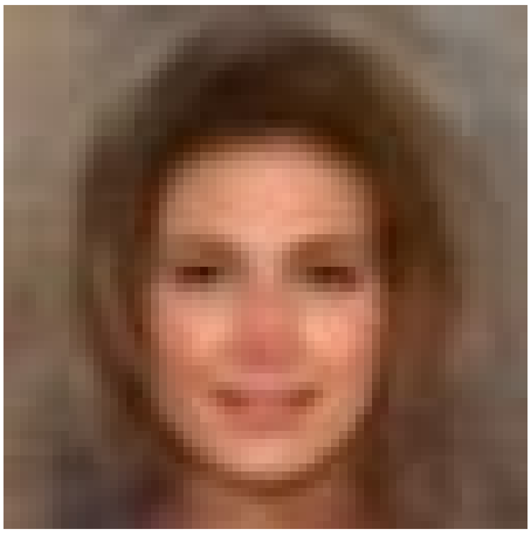
(d) celebA data: SDGM reconstruction

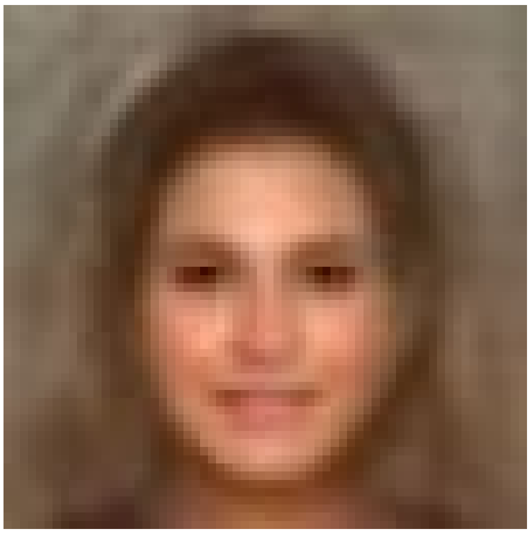
(e) celebA data: Householder flow (1 transformation) reconstruction

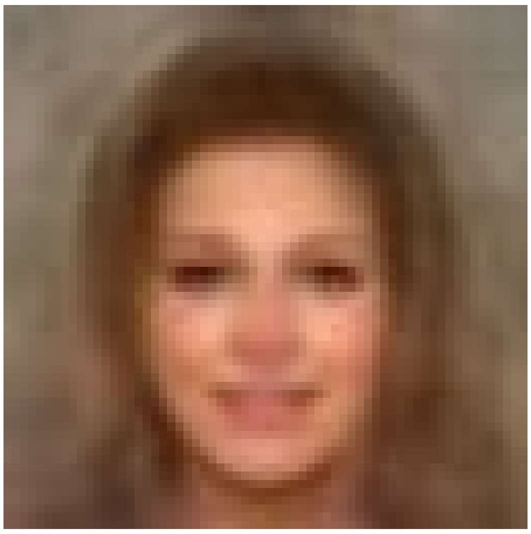
(f) celebA data: Householder flow (10 transformations) reconstruction

Fig. 5.4 celebA data: Reconstruction of a single sample from the tests dataset under several models. All models only use a single Monte Carlo sample for expectations.

(a) celebA data: VAE sample

(b) celebA data: IWAE sample

(c) celebA data: ADGM sample

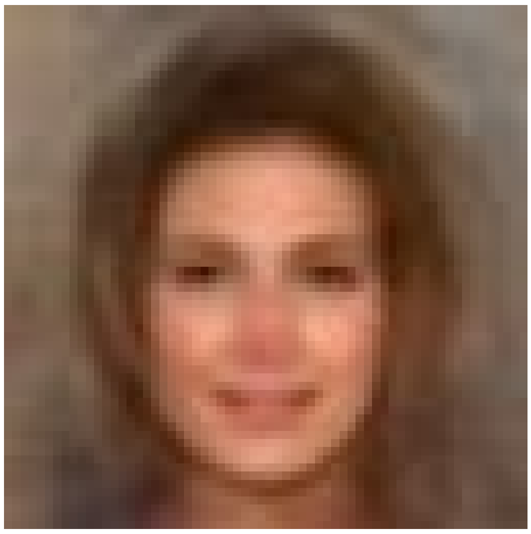
(d) celebA data: SDGM sample

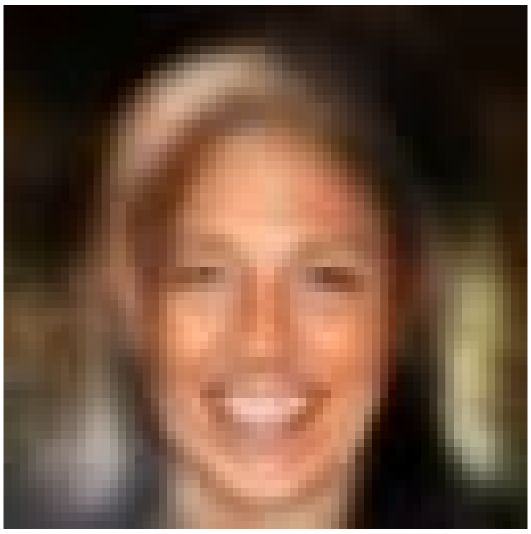
(e) celebA data: Householder flow (1 transformation) sample

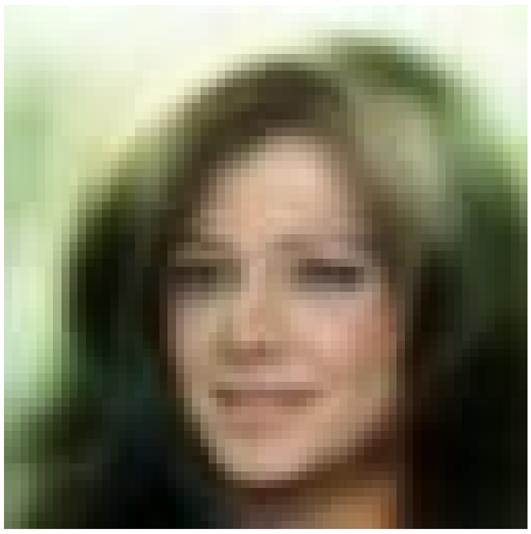
(f) celebA data: Householder flow (10 transformations) sample

Fig. 5.5 celebA data: Sampling from models. All models only use a single Monte Carlo sample for expectations.

5.4 Pose Timing

In this section, we examine how long key steps of the modeling process take. In particular, we will consider how long a particular model takes to encode a data-point, decode a latent point, and update the network parameters. Additionally, for encoding and decoding, we consider the time taken when using Chainer *volatile* and *non-volatile* variables. With non-volatile variables, the history of operations used to create that variable is not stored. This prevents that variable from being updated but also saves on memory usage. We record the timings on volatile and non-volatile variables to compare the difference in encoding and decoding between a training and testing scenario. This was done for 100 epochs and the average is reported along with the standard deviation.

5.4.1 Results

Number of Monte Carlo Samples	Training			Validation	
	Encoding	Decoding	Update	Encoding	Decoding
1	0.0076 (± 0.03913)	0.0036 (± 0.00101)	0.0095 (± 0.01733)	0.0035 (± 0.00033)	0.0035 (± 0.00177)
2	0.0038 (± 0.00134)	0.0033 (± 0.00187)	0.0126 (± 0.00454)	0.0038 (± 0.00051)	0.0034 (± 0.00077)
5	0.0036 (± 0.00188)	0.0034 (± 0.00047)	0.0245 (± 0.00350)	0.0033 (± 0.00213)	0.0033 (± 0.00068)

Table 5.30 Pose data: average times over the training and validation set (351,275 and 175,638 samples respectively). We also report the standard deviation in brackets. Model examined is the VAE.

Number of Monte Carlo Samples	Training			Validation	
	Encoding	Decoding	Update	Encoding	Decoding
1	0.0037 (± 0.00129)	0.0034 (± 0.00018)	0.0087 (± 0.00074)	0.0034 (± 0.00033)	0.0033 (± 0.00070)
2	0.0037 (± 0.00142)	0.0033 (± 0.00028)	0.0154 (± 0.00150)	0.0036 (± 0.00052)	0.0034 (± 0.00059)
5	0.0037 (± 0.00138)	0.0033 (± 0.00026)	0.0325 (± 0.00278)	0.0037 (± 0.00106)	0.0033 (± 0.00041)

Table 5.31 Pose data: average times over the training and validation set (351,275 and 175,638 samples respectively). We also report the standard deviation in brackets. Model examined is the IWAE.

Model	Training			Validation	
	Encoding	Decoding	Update	Encoding	Decoding
ADGM	0.0086 (± 0.01838)	0.0065 (± 0.00203)	0.2474 (± 0.00306)	0.0069 (± 0.00060)	0.0065 (± 0.00077)
SDGM	0.0068 (± 0.00198)	0.0064 (± 0.00452)	0.2467 (± 0.00330)	0.0070 (± 0.00058)	0.0065 (± 0.00051)

Table 5.32 Pose data: average times over the training and validation set (351,275 and 175,638 samples respectively). We also report the standard deviation in brackets. Models examined are the ADGM and SDGM. A single Monte Carlo sample was used for the expectation.

Number of Transformations	Training			Validation	
	Encoding	Decoding	Update	Encoding	Decoding
1	0.0041 (± 0.00126)	0.0073 (± 0.01774)	0.0110 (± 0.00132)	0.0039 (± 0.00101)	0.0051 (± 0.00095)
10	0.0046 (± 0.00498)	0.0229 (± 0.01109)	0.0220 (± 0.00825)	0.0036 (± 0.00342)	0.0182 (± 0.01264)

Table 5.33 Pose data: average times over the training and validation set (351,275 and 175,638 samples respectively). We also report the standard deviation in brackets. Model examined is the Householder flow. A single Monte Carlo sample was used for the expectation.

Number of Transformations	Training			Validation	
	Encoding	Decoding	Update	Encoding	Decoding
1	0.0040 (± 0.00171)	0.0077 (± 0.00068)	0.0102 (± 0.00152)	0.0036 (± 0.00144)	0.0074 (± 0.00220)
2	0.0044 (± 0.00654)	0.0107 (± 0.00801)	0.0123 (± 0.01152)	0.0025 (± 0.01193)	0.0091 (± 0.00970)
3	0.0028 (± 0.00913)	0.0128 (± 0.01430)	0.0117 (± 0.01518)	0.0041 (± 0.01632)	0.0114 (± 0.01879)
4	0.0041 (± 0.00183)	0.0169 (± 0.00154)	0.1326 (± 0.00275)	0.0038 (± 0.00081)	0.0150 (± 0.00168)
8	0.0041 (± 0.00140)	0.0277 (± 0.00203)	0.1397 (± 0.00293)	0.0038 (± 0.00131)	0.0255 (± 0.00335)

Table 5.34 Pose data: average times over the training and validation set (351,275 and 175,638 samples respectively). We also report the standard deviation in brackets. Model examined is the IAF. A single Monte Carlo sample was used for the expectation.

5.4.2 Discussion

We first consider the times taken by the VAE and IWAE models, shown in Table 5.30 and 5.31. As they have the same architectures, it is not surprising to see that the time taken to encode a data-point for both these models is approximately the same. This same can be observed for the time taken to decode latent points. We note that this time is averaged across the number of MC samples used which is why there isn't any significant increase in time as the number of MC samples is increased.

For both the VAE and IWAE model, we observe that the time taken to update the network parameters increases as the number of MC samples used increases. Using more samples results in a more complex computational graph and this results in a more involved backpropagation update procedure. As the update procedure takes into account the loss function or ELBO being used, we can compare differences between the VAE and IWAE here. Using only a single MC sample, the IWAE objective is almost the same as the VAE objective. The only difference for this case is that with the VAE, we evaluate the KL divergence analytically but for the IWAE, we use expectations. In our code, the analytic KL is implemented as a separate function whereas for the IWAE, it is evaluated closer to the other operations. This may explain why the update time is longer for the VAE compared to the IWAE when only a single MC sample is used. When using 2 or 5 MC samples, the complexity of the IWAE ELBO comes into play and we see that for both theses cases, updates take longer compared to the VAE.

It is also interesting to note that while non-volatile variables consume less memory and hence should be faster to encode and decode, we observe no difference. If the data-points and latent points had more dimensions or if we used larger batch sizes, perhaps a difference would show since we would be increasing the memory consumption. However, for our investigation into the VAE and IWAE models on the Pose dataset, there was no difference between using volatile and non-volatile variables with respect to encoding and decoding time.

Next we consider the timings recorded for the ADGM and SDGM models, as shown in Table 5.32. We begin by noting that the times taken to encode are similar whether using volatile or non-volatile variables, for both the models. The only value that is a little higher than the others is the volatile encoding time for the ADGM. However, the significantly higher standard deviation means that this measure may not be a good representative for the average ADGM encoding time. Once again, the update timings hold more interesting information. If we consider their probabilistic models, they both have the same variables with the key difference being in how these variables relate to each other. Therefore, from a network perspective, the number of parameters in both networks is approximately the same and with a single MC sample, so is the number of computations. As a result, their update times are approximately the same.

For the Householder flow model, we defined the encoding process to only encapsulate the time taken to go from the original data-point to the basic latent space, z_0. This is why the time taken to encode is approximately the same whether a single transformation or 10 are used as shown in Table 5.33. The additional transformation or flows are timed as part of the decoding process and hence we see that for both the training and validation set, there is an increase in decoding time when more transformations are used. Note that even though 9 more transformations are used, we don't see the time increase by a factor of 10. This is because there are operations involved in the decoding process that are present in the same amount regardless of how many transformations are used. Specifically, after the latent point has been transformed, it must be pushed through the decoder network to obtain the reconstructed data-point. This aspect of the decoding process will occur in the same manner regardless of how many flows were applied to transform the latent point. Additionally, as more flows are used, there are more operations involved which leads to a longer update period. Note that with the Householder flow, the same linear layer is used to obtain a new Householder vector for each flow. This means that more flows don't change the number of parameters of the network. The longer update time is due to the increase in number of operations, not the number of parameters.

Considering the IAF models, the same idea was applied to timing the encoding and decoding procedure as was done with the Householder model. The encoding procedure times how long it takes to encode a data-point to the basic latent space. The decoding time covers the time taken to apply the auto-regressive flows to the first latent point and also the time taken to decode the final latent point to the reconstructed data-point. Hence we see the encoding time remain approximately the same regardless of how many flows are used while the decoding time increases as more flows are applied. For the IAF model, each transformations is categorized by a different set of parameters. Therefore the increase in update time is due to both an increase in the number of operations in the gradient calculation and also an increase in the number of parameters to update.

Having considered the different models in relative isolation, we now compare the timings across all the models on the Pose data. Firstly, encoding takes about the same amount of time for the different models. The only two models that have a longer encoding procedure are the ADGM and SDGM. However, these models have an additional variable in the probabilistic model. This additional variable and the parameters associated with it would explain why the encoding procedure for the ADGM and SDGM take much longer than the other models.

Next, we examine the decoding procedure across these different models. The VAE and IWAE models have the fastest times here as they have the simplest decoding procedure. The ADGM and SDGM also have fairly standard decoding procedures, in that they do not have to consider number of transformations or flows like the Householder or IAF model. However, as both the ADGM and SDGM have more complex generative models, their decoding procedures are also more involved. As a result, their decoding takes significantly longer than the VAE or IWAE. As mentioned previously, for the Householder and IAF model, using more transformations increases the decoding time. However, even with just a single transformation, these models take longer to decode compared to the other models. If we compare the time taken to decode for the Householder model against the IAF model, we see that IAF transformations are more costly in terms of time. Using 8 IAF transformations takes longer than using 10 Householder flow transformations. Hence when it comes to decoding, the IAF model has the highest cost.

Following on, we look at the time taken to update the model after a batch has been processed. This metric is very informative as it relates to the computational graph of each model and hence the complexity of these models. It can also act as a proxy as to how many parameters a particular configuration has. The higher the number of parameters, the longer the update procedure will take. This may not always be the case and we elaborate on this further on. Firstly, given a single MC sample, we see that the the VAE and IWAE models take a shorter time to update than the other models. As previously noted, these models have the simplest architectures and hence it is unsurprising that these models update quickly, relative to the other models. Even though the ADGM and SDGM may have less network parameters and less operations compared to the flow models, the underlying probabilistic model is more complex and hence these two models have a very high update time. Comparing the flow models, we see that the update time increases at a much faster rate for the IAF model compared to the Householder flow model as more transformations are added. As previously mentioned, more transformations with the Householder flow do not lead to more parameters unlike the IAF. Thus when increasing the number of transformations with an IAF model, the number of operations and number of parameters increases leading to a larger update time compared to the Householder flow model in which only the number of operations increases. Overall, the ADGM and SDGM model have the highest base update time. We include the term 'base' as it is possible that by using an even higher number of transformations with the Householder flow or IAF model compared to what was considered here, their respective update times might exceed that of the ADGM and SDGM.

5.5 MNIST Timing

5.5.1 Results

Number of Monte Carlo Samples	Training			Validation	
	Encoding	Decoding	Update	Encoding	Decoding
1	0.0020 (± 0.00224)	0.0014 (± 0.00007)	0.0133 (± 0.00180)	0.0018 (± 0.00024)	0.0014 (± 0.00014)
2	0.0019 (± 0.00222)	0.0013 (± 0.00051)	0.0198 (± 0.00148)	0.0017 (± 0.00007)	0.0013 (± 0.00004)
5	0.0020 (± 0.00227)	0.0013 (± 0.00034)	0.0395 (± 0.00196)	0.0017 (± 0.00009)	0.0013 (± 0.00006)

Table 5.35 MNIST data: average times over the training and validation set (50,000 and 10,000 samples respectively). We also report the standard deviation in brackets. Model examined is the VAE.

Number of Monte Carlo Samples	Training			Validation	
	Encoding	Decoding	Update	Encoding	Decoding
1	0.0020 (± 0.00212)	0.0013 (± 0.00060)	0.0132 (± 0.00141)	0.0018 (± 0.00024)	0.0013 (± 0.00005)
2	0.0020 (± 0.00218)	0.0014 (± 0.00007)	0.0198 (± 0.00182)	0.0017 (± 0.00006)	0.0014 (± 0.00005)
5	0.0019 (± 0.00236)	0.0014 (± 0.00004)	0.0395 (± 0.00231)	0.0017 (± 0.00015)	0.0014 (± 0.00011)

Table 5.36 MNIST data: average times over the training and validation set (50,000 and 10,000 samples respectively). We also report the standard deviation in brackets. Model examined is the IWAE.

Model	Training			Validation	
	Encoding	Decoding	Update	Encoding	Decoding
ADGM	0.0039 (± 0.00226)	0.0031 (± 0.00091)	0.0257 (± 0.00180)	0.0031 (± 0.00386)	0.0031 (± 0.00010)
SDGM	0.0036 (± 0.00238)	0.0032 (± 0.00067)	0.0241 (± 0.00149)	0.0036 (± 0.00012)	0.0028 (± 0.00393)

Table 5.37 MNIST data: average times over the training and validation set (50,000 and 10,000 samples respectively). We also report the standard deviation in brackets. Models examined are the ADGM and SDGM. A single Monte Carlo sample was used for the expectation.

Number of Transformations	Training			Validation	
	Encoding	Decoding	Update	Encoding	Decoding
1	0.0022 (± 0.00220)	0.0028 (± 0.00043)	0.0211 (± 0.00136)	0.0020 (± 0.00022)	0.0027 (± 0.00020)
10	0.0022 (± 0.00166)	0.0158 (± 0.00169)	0.0789 (± 0.00308)	0.0020 (± 0.00026)	0.0152 (± 0.00158)

Table 5.38 MNIST data: average times over the training and validation set (50,000 and 10,000 samples respectively). We also report the standard deviation in brackets. Model examined is the Householder flow. A single Monte Carlo sample was used for the expectation.

5.5.2 Discussion

For most of the models, we observe the same trends and behaviours for the MNIST dataset as was seen with the Pose data. There are a few subtle differences between the results on these two datasets. To begin with, the models took longer to encode and decode the Pose datasets compared to MNIST. We believe that this is due to the size of the mini-batches being used. Preliminary experiments showed that the GPU processes ran slower when the load was higher, even if the entire capacity of the GPU was not being utilized. With the Pose timing experiments, we used a batch size of 16,384 whereas with MNIST, we used 4,096. The larger batch size of the Pose data appears to have taken slightly longer to encode and decode compared to the MNIST dataset. It is also interesting to note that the batch size seemed to have a greater effect that the dimensionality of the data since with MNIST, the dimensionality of the original data-points and the dimensionality of the latent space were far greater compared to their respective counterparts in the Pose dataset. However, while using larger batches incurs a small time cost, the time saved from having to process less batches is far greater. Therefore, to minimize the overall time overhead, large batch sizes should be used despite having a longer encoding and decoding process per batch.

We see that the VAE and IWAE model take less time to encode, decode, and update due to their simpler architectures. Additionally, the difference in update time between the VAE and IWAE are much smaller here. We believe that this is because the batch sizes were significantly smaller. A larger batch size will likely show the IWAE model taking longer than the VAE model as more MC samples are used. While the ADGM and SDGM have large base times, we see that if we use 10 Householder flow transformations, the decoding and update time of the Householder model is greater than those of the ADGM and SDGM.

5.6 celebA Timing

5.6.1 Results

Number of Monte Carlo Samples	Training			Validation	
	Encoding	Decoding	Update	Encoding	Decoding
1	0.0038 (± 0.00210)	0.0029 (± 0.00005)	0.1953 (± 0.00069)	0.0036 (± 0.00009)	0.0028 (± 0.00006)
2	0.0036 (± 0.00186)	0.0028 (± 0.00011)	0.3233 (± 0.02761)	0.0034 (± 0.00015)	0.0027 (± 0.00010)
5	0.0040 (± 0.00073)	0.0048 (± 0.00070)	0.6652 (± 0.00088)	0.0040 (± 0.00024)	0.0032 (± 0.00018)

Table 5.39 celebA data: average times over the training and validation set (100,000 and 50,000 samples respectively). We also report the standard deviation in brackets. Model examined is the VAE.

Number of Monte Carlo Samples	Training			Validation	
	Encoding	Decoding	Update	Encoding	Decoding
1	0.0037 (± 0.00204)	0.0029 (± 0.00006)	0.1954 (± 0.00086)	0.0035 (± 0.00007)	0.0028 (± 0.00005)
2	0.0037 (± 0.00199)	0.0029 (± 0.00005)	0.3136 (± 0.00099)	0.0035 (± 0.00007)	0.0028 (± 0.00006)
5	0.0037 (± 0.00207)	0.0030 (± 0.00007)	0.6672 (± 0.00081)	0.0035 (± 0.00010)	0.0028 (± 0.00006)

Table 5.40 celebA data: average times over the training and validation set (100,000 and 50,000 samples respectively). We also report the standard deviation in brackets. Model examined is the IWAE.

Model	Training			Validation	
	Encoding	Decoding	Update	Encoding	Decoding
ADGM	0.0071 (± 0.00204)	0.0062 (± 0.00011)	0.3307 (± 0.00095)	0.0069 (± 0.00015)	0.0061 (± 0.00012)
SDGM	0.0072 (± 0.00291)	0.0062 (± 0.00012)	0.2837 (± 0.00069)	0.0069 (± 0.00016)	0.0061 (± 0.00011)

Table 5.41 celebA data: average times over the training and validation set (100,000 and 50,000 samples respectively). We also report the standard deviation in brackets. Models examined are the ADGM and SDGM. A single Monte Carlo sample was used for the expectation.

Number of Transformations	Training			Validation	
	Encoding	Decoding	Update	Encoding	Decoding
1	0.0039 (± 0.00208)	0.0043 (± 0.00037)	0.2193 (± 0.00074)	0.0037 (± 0.00007)	0.0041 (± 0.00008)
10	0.0037 (± 0.00216)	0.0158 (± 0.00075)	0.3907 (± 0.00078)	0.0035 (± 0.00022)	0.0151 (± 0.00047)

Table 5.42 celebA data: average times over the training and validation set (100,000 and 50,000 samples respectively). We also report the standard deviation in brackets. Model examined is the Householder flow. A single Monte Carlo sample was used for the expectation.

5.6.2 Discussion

The celebA dataset was the largest dataset considered in terms of disk space usage. The machine used to run the timing experiments for the Pose and MNIST datasets was too small to keep the celebA dataset on disk. Therefore, timing experiments for the celebA dataset were run on a different machine with a different GPU. As such, we cannot make direct comparisons between the times recorded for the celebA dataset against those for the Pose and MNIST datasets. However, the results gathered are still useful for checking if the trends observed when timing the Pose and MNIST dataset experiments still hold. In general, the same trends are observed. The VAE and IWAE model take the least amount of time to encode, decode, and update. While the ADGM and SDGM take a lot of time, if a sufficient number of Householder flow transformations are applied, the decoding and update time taken by the Householder model exceeds that of the ADGM and SDGM.

5.7 Practical Recommendations

In the previous sections, we discussed the modeling capacity of each of our models as well as the time costs associated with them. The SDGM performed consistently well across all tasks with regards to ELBO but often took significantly longer to carry out its operations (encode, decode and update) as opposed to the other options. For the Pose data, we recommend the IAF as it performed the best and had smaller training times, even with 8 transformations, relative to other models like the SDGM. Computational resources permitting, we recommend using more transformations.

While the SDGM model had the best ELBO on the MNIST and celebA datasets, the IWAE model with 5 MC samples also performed very well while having shorter encoding and decoding times. On the MNIST dataset, the ELBO gap between the SDGM and IWAE 5 MC model is small enough that if fast models were a priority, both from a training and sampling perspective, the IWAE 5 MC model would be a good option. We observe that for the update procedure on the celebA dataset, the SDGM model requires less time compared to the IWAE 5 MC model which makes the SDGM more favourable in this situation. Speaking more generally, the IWAE model requires more samples to achieve a better fit but the increased update time cost associated with this is strongly linked to the dataset being modeled. For low dimensional data like MNIST, we see that the update time doesn't increase much as more MC samples are used but for higher dimensional data like celebA, we see the update time increase at a much faster rate. This is not as big an issue with the SDGM model since it is capable of achieving good fits without using more than 1 MC sample. If small training and sampling times are not a priority, we recommend using the SDGM. However, if these are bigger priorities than the ELBO, we recommend considering the IWAE model. Choosing the right setup with the IWAE model may be more involved as we have to consider the dimensionality of the data and choose the appropriate number of MC samples. More MC samples will lead to a better ELBO but at some point, the time savings that were important are lost.

Chapter 6

Summary and Future Work

6.1 Summary

In conclusion, we believe that we achieved the aims of this project. In Chapter 5, we provided a thorough comparison of several modifications to the Variational Auto-Encoder (VAE) ([31, 54]). We measured the variational lower bound as is common to most of the literature but additionally we reported the time taken for different stages of the modeling process. Using both these metrics, in Section 5.7, we offered practical guidelines on the which models might be best suited for different tasks. Additionally, while most related work focuses on MNIST, we also looked at two different datasets: celebA and Pose (MSRC-12). By showing recurring trends across three significantly different datasets, we are able to state our conclusions with more confidence. On top of this, we have also contributed an extensive Chainer code repository ([16]) to allow others access to these new probabilistic deep generative models and to replicate our experiments.

6.2 Future Work and Extensions

6.2.1 Inverse Autoregressive Flow on other datasets

We were unable to obtain results for the Inverse Autoregressive Flow (IAF) model on the MNIST and celebA datasets. While we could draw some conclusions about this model based on its performance on the Pose dataset, [33] claimed that one of the main strengths of the IAF model was its ability to handle high dimensional latent spaces. Of the datasets examined, the Pose dataset involved the latent space with the smallest dimension, compared to MNIST and celebA. To fully examine the capabilities of the IAF model, we believe that it will be necessary to examine its performance on datasets requiring large latent spaces.

6.2.2 Planar Flow model

We attempted to implement the Planar flow model which was the focus of [53] but were unsuccessful. Our attempted implementation has been included in the aforementioned repository. We believe that this is another important model to investigate as it was one of the first normalizing flow methods examined. It would be especially useful to compare the performance of this model against that of the Householder flow and IAF models as these latter two are more recent normalizing flow models.

Specifically, [33] claimed that the Planar flow model was analogous to a multi-layer perceptron bottleneck and would perform poorly when handling high-dimensional latent spaces whereas the IAF overcame this issue. It would be useful to test this claim, specifically to determine at which point the latent space became too large to be modeled by the Planar flow model.

The Householder flow model by [67] is an example of a volume preserving normalizing flow as opposed to the Planar flow model which is a general normalizing flow model. The former is cheaper than the latter and by implementing the Planar flow model, we would be better able to consider the trade-off between computational complexity and accuracy between general and volume preserving normalizing flows.

6.2.3 Timing of celebA dataset

As mentioned in Section 5.6.2, due to the size of the celebA dataset, a different machine had to be used to carry out the timing experiments compared to the Pose and MNIST datasets. It would be beneficial to redo the celebA timing experiments using the same GPU model used for the other datasets but with a machine with enough disk space to store the dataset. The results of this would provide more insight into the relationship between timing and data dimensionality as the celebA dataset datapoints were of a much larger dimension than the Pose and MNIST datasets.

6.2.4 Fine-tuning models

In this work, none of the model architectures were fine-tuned extensively. For the Pose and MNIST datasets, related work informed our model choice. For the celebA dataset, we considered the literature and performed experiments with the validation dataset and the VAE model to determine the best architecture choice. However, to better measure the capacity of each model, we should instead carry out the architecture experiments on the validation dataset for each model individually. In this work, we assumed that the architecture and settings used for the VAE model were also suitable for the other models but this might not necessarily be true. We do not believe that in being more thorough with the architecture choice, the results obtained and trends observed will be significantly different but instead, we could be more secure about our observations and recommendations.

6.2.5 Convolutional layers

As discussed in Section 5.3.3, our models encountered difficulty in reconstructing images from the celebA test dataset even though sampling from the generative network indicated that facial attributes were being learned. To overcome this issue, we would recommend experimenting with convolutional layers instead of fully connected layers. These layers have shown a lot of promise in extracting meaningful features for complex image data ([34, 52]).

6.2.6 Depth in stochastic layers

One model that performed consistently well across all the datasets was the Skip Deep Generative Model (SDGM). As mentioned in Section 5.1.3, we believe that this is due to the depth in the stochastic layer. Having more than one layer in the latent space is not something unique to the SDGM. Hence it would be worthwhile to increase the stochastic depth for the other models and examine the resulting performance. Such an undertaking would provide clearer understanding into the importance and limitations of increasing the depth of the latent space.

References

[1] S. Agrawal and A. Dukkipati. Deep variational inference without pixel-wise reconstruction. *arXiv preprint arXiv:1611.05209*, 2016.

[2] Y. Bengio. Neural net language models. *Scholarpedia*, 3(1):3881, 2008.

[3] Y. Bengio, Y. LeCun, et al. Scaling learning algorithms towards ai. *Large-scale kernel machines*, 34(5):1–41, 2007.

[4] Y. Bengio, A. Courville, and P. Vincent. Representation learning: A review and new perspectives. *IEEE transactions on pattern analysis and machine intelligence*, 35(8): 1798–1828, 2013.

[5] M. Bicego, A. Lagorio, E. Grosso, and M. Tistarelli. On the use of sift features for face authentication. In *Computer Vision and Pattern Recognition Workshop, 2006. CVPRW'06. Conference on*, pages 35–35. IEEE, 2006.

[6] A. W. Black. Clustergen: A statistical parametric synthesizer using trajectory modeling. In *Ninth International Conference on Spoken Language Processing*, 2006.

[7] D. M. Blei. Variational inference.

[8] D. M. Blei, A. Kucukelbir, and J. D. McAuliffe. Variational inference: A review for statisticians. *Journal of the American Statistical Association*, (just-accepted), 2017.

[9] A. E. Bryson. *Applied optimal control: optimization, estimation and control*. CRC Press, 1975.

[10] Y. Burda, R. Grosse, and R. Salakhutdinov. Importance weighted autoencoders. *arXiv preprint arXiv:1509.00519*, 2015.

[11] L. Cai, H. Gao, and S. Ji. Multi-stage variational auto-encoders for coarse-to-fine image generation. *arXiv preprint arXiv:1705.07202*, 2017.

[12] Chervinskii. Auto-encoder structure, 2015. URL https://commons.wikimedia.org/wiki/File:Autoencoder_structure.png.

[13] D. Ciregan, U. Meier, and J. Schmidhuber. Multi-column deep neural networks for image classification. In *Computer Vision and Pattern Recognition (CVPR), 2012 IEEE Conference on*, pages 3642–3649. IEEE, 2012.

[14] D. C. Cireşan, U. Meier, L. M. Gambardella, and J. Schmidhuber. Deep, big, simple neural nets for handwritten digit recognition. *Neural computation*, 22(12):3207–3220, 2010.

[15] C. Cremer, Q. Morris, and D. Duvenaud. Reinterpreting importance-weighted autoencoders. *arXiv preprint arXiv:1704.02916*, 2017.

[16] A. D. D'Cruz. Deep generative models. https://github.com/ashwindcruz/dgm, 2017.

[17] C. Doersch. Tutorial on variational autoencoders. *arXiv preprint arXiv:1606.05908*, 2016.

[18] J. Duchi, E. Hazan, and Y. Singer. Adaptive subgradient methods for online learning and stochastic optimization. *Journal of Machine Learning Research*, 12(Jul):2121–2159, 2011.

[19] S. Fothergill, H. Mentis, P. Kohli, and S. Nowozin. Instructing people for training gestural interactive systems. In *Proceedings of the SIGCHI Conference on Human Factors in Computing Systems*, pages 1737–1746. ACM, 2012.

[20] K. Fukushima and S. Miyake. Neocognitron: A self-organizing neural network model for a mechanism of visual pattern recognition. In *Competition and cooperation in neural nets*, pages 267–285. Springer, 1982.

[21] M. Gales. 4f10 deep learning. 2016. URL http://mi.eng.cam.ac.uk/~mjfg/local/4F10/index.html.

[22] T. Ganchev, N. Fakotakis, and G. Kokkinakis. Comparative evaluation of various mfcc implementations on the speaker verification task. In *Proceedings of the SPECOM*, volume 1, pages 191–194, 2005.

[23] M. Germain, K. Gregor, I. Murray, and H. Larochelle. Made: masked autoencoder for distribution estimation. In *Proceedings of the 32nd International Conference on Machine Learning (ICML-15)*, pages 881–889, 2015.

[24] Z. Ghahramani. Unsupervised learning. In *Advanced lectures on machine learning*, pages 72–112. Springer, 2004.

[25] X. Hou, L. Shen, K. Sun, and G. Qiu. Deep feature consistent variational autoencoder. In *Applications of Computer Vision (WACV), 2017 IEEE Winter Conference on*, pages 1133–1141. IEEE, 2017.

[26] D. H. Hubel and T. N. Wiesel. Receptive fields, binocular interaction and functional architecture in the cat's visual cortex. *The Journal of physiology*, 160(1):106–154, 1962.

[27] S. Ioffe and C. Szegedy. Batch normalization: Accelerating deep network training by reducing internal covariate shift. In *International Conference on Machine Learning*, pages 448–456, 2015.

[28] E. Jang. A beginner's guide to variational methods: Mean-field approximation, 2016. URL http://blog.evjang.com/2016/08/variational-bayes.html.

[29] A. Karpathy. Cs231n convolutional neural networks for visual recognition, 2017. URL http://cs231n.github.io.

[30] D. Kingma and J. Ba. Adam: A method for stochastic optimization. *arXiv preprint arXiv:1412.6980*, 2014.

[31] D. P. Kingma and M. Welling. Auto-encoding variational bayes. *arXiv preprint arXiv:1312.6114*, 2013.

[32] D. P. Kingma, S. Mohamed, D. J. Rezende, and M. Welling. Semi-supervised learning with deep generative models. In *Advances in Neural Information Processing Systems*, pages 3581–3589, 2014.

[33] D. P. Kingma, T. Salimans, and M. Welling. Improving variational inference with inverse autoregressive flow. *arXiv preprint arXiv:1606.04934*, 2016.

[34] A. Krizhevsky, I. Sutskever, and G. E. Hinton. Imagenet classification with deep convolutional neural networks. In *Advances in neural information processing systems*, pages 1097–1105, 2012.

[35] H. Larochelle, D. Erhan, A. Courville, J. Bergstra, and Y. Bengio. An empirical evaluation of deep architectures on problems with many factors of variation. In *Proceedings of the 24th international conference on Machine learning*, pages 473–480. ACM, 2007.

[36] A. B. L. Larsen, S. K. Sønderby, H. Larochelle, and O. Winther. Autoencoding beyond pixels using a learned similarity metric. *arXiv preprint arXiv:1512.09300*, 2015.

[37] Y. LeCun. The mnist database of handwritten digits. *http://yann. lecun. com/exdb/mnist/*, 1998.

[38] Y. LeCun, Y. Bengio, and G. Hinton. Deep learning. *Nature*, 521(7553):436–444, 2015.

[39] Z. Liu, P. Luo, X. Wang, and X. Tang. Deep learning face attributes in the wild. In *Proceedings of International Conference on Computer Vision (ICCV)*, 2015.

[40] L. Maaløe, C. K. Sønderby, S. K. Sønderby, and O. Winther. Auxiliary deep generative models. *arXiv preprint arXiv:1602.05473*, 2016.

[41] D. J. MacKay. Local minima, symmetry-breaking, and model pruning in variational free energy minimization. *Inference Group, Cavendish Laboratory, Cambridge, UK*, 2001.

[42] W. S. McCulloch and W. Pitts. A logical calculus of the ideas immanent in nervous activity. *Bulletin of mathematical biology*, 52(1):99–115, 1990.

[43] L. Mescheder, S. Nowozin, and A. Geiger. Adversarial variational bayes: Unifying variational autoencoders and generative adversarial networks. *arXiv preprint arXiv:1701.04722*, 2017.

[44] Microsoft. Msrc-12, 2012. URL https://www.microsoft.com/en-us/download/details.aspx?id=52283.

[45] V. Nair and G. E. Hinton. Rectified linear units improve restricted boltzmann machines. In *Proceedings of the 27th international conference on machine learning (ICML-10)*, pages 807–814, 2010.

[46] K. S. Narendra and M. A. Thathachar. Learning automata-a survey. *IEEE Transactions on systems, man, and cybernetics*, (4):323–334, 1974.

[47] M. A. Nielsen. *Chapter 2: How the backpropagation algorithm works*. Determination Press, 2015. URL http://neuralnetworksanddeeplearning.com/chap2.html.

[48] A. v. d. Oord, S. Dieleman, H. Zen, K. Simonyan, O. Vinyals, A. Graves, N. Kalchbrenner, A. Senior, and K. Kavukcuoglu. Wavenet: A generative model for raw audio. *arXiv preprint arXiv:1609.03499*, 2016.

[49] A. v. d. Oord, N. Kalchbrenner, and K. Kavukcuoglu. Pixel recurrent neural networks. *arXiv preprint arXiv:1601.06759*, 2016.

[50] J. Paisley, D. Blei, and M. Jordan. Variational bayesian inference with stochastic search. *arXiv preprint arXiv:1206.6430*, 2012.

[51] C. Poultney, S. Chopra, Y. L. Cun, et al. Efficient learning of sparse representations with an energy-based model. In *Advances in neural information processing systems*, pages 1137–1144, 2007.

[52] A. Radford, L. Metz, and S. Chintala. Unsupervised representation learning with deep convolutional generative adversarial networks. *arXiv preprint arXiv:1511.06434*, 2015.

[53] D. J. Rezende and S. Mohamed. Variational inference with normalizing flows. *arXiv preprint arXiv:1505.05770*, 2015.

[54] D. J. Rezende, S. Mohamed, and D. Wierstra. Stochastic backpropagation and approximate inference in deep generative models. *arXiv preprint arXiv:1401.4082*, 2014.

[55] F. Rosenblatt. The perceptron: A probabilistic model for information storage and organization in the brain. *Psychological review*, 65(6):386, 1958.

[56] D. E. Rumelhart, G. E. Hinton, and R. J. Williams. Learning internal representations by error propagation. Technical report, California Univ San Diego La Jolla Inst for Cognitive Science, 1985.

[57] R. Salakhutdinov. *Learning deep generative models*. University of Toronto, 2009.

[58] J. Schmidhuber. Deep learning in neural networks: An overview. *Neural networks*, 61: 85–117, 2015.

[59] F. Seide, G. Li, and D. Yu. Conversational speech transcription using context-dependent deep neural networks. In *Twelfth Annual Conference of the International Speech Communication Association*, 2011.

[60] W. Shang, K. Sohn, D. Almeida, and H. Lee. Understanding and improving convolutional neural networks via concatenated rectified linear units. *CoRR*, abs/1603.05201, 2016. URL http://arxiv.org/abs/1603.05201.

[61] P. Y. Simard, D. Steinkraus, J. C. Platt, et al. Best practices for convolutional neural networks applied to visual document analysis. In *ICDAR*, volume 3, pages 958–962, 2003.

[62] C. K. Sønderby, T. Raiko, L. Maaløe, S. K. Sønderby, and O. Winther. How to train deep variational autoencoders and probabilistic ladder networks. *arXiv preprint arXiv:1602.02282*, 2016.

[63] E. Tabak and C. V. Turner. A family of nonparametric density estimation algorithms. *Communications on Pure and Applied Mathematics*, 66(2):145–164, 2013.

[64] E. G. Tabak, E. Vanden-Eijnden, et al. Density estimation by dual ascent of the log-likelihood. *Communications in Mathematical Sciences*, 8(1):217–233, 2010.

[65] T. Tieleman and G. Hinton. Lecture 6.5-rmsprop: Divide the gradient by a running average of its recent magnitude. *COURSERA: Neural networks for machine learning*, 4(2):26–31, 2012.

[66] S. Tokui, K. Oono, S. Hido, and J. Clayton. Chainer: a next-generation open source framework for deep learning. In *Proceedings of workshop on machine learning systems (LearningSys) in the twenty-ninth annual conference on neural information processing systems (NIPS)*, volume 5, 2015.

[67] J. M. Tomczak and M. Welling. Improving variational auto-encoders using householder flow. *arXiv preprint arXiv:1611.09630*, 2016.

[68] S. Zagoruyko and N. Komodakis. Wide residual networks. *arXiv preprint arXiv:1605.07146*, 2016.

[69] H. Zhou, Y. Yuan, and C. Shi. Object tracking using sift features and mean shift. *Computer vision and image understanding*, 113(3):345–352, 2009.